Mapping clay content variation using electromagnetic induction techniques

J. Triantafilis[a,*], S.M. Lesch[b]

[a] *School of Biological, Earth and Environmental Sciences, The University of New South Wales, NSW 2052, Australia*
[b] *George E. Brown Jr. Salinity Laboratory, 450 West Big Springs Road, Riverside, CA 92507, USA*

Abstract

Effective management of the soil resource requires basic information about the spatial distribution of various attributes. A method widely used for providing spatial information is a combination of sampling strategies and geostatistics. However, geostatistical methods demand intensive sampling that is expensive and time-consuming. Geophysical methods, such as electromagnetic (EM) induction, offer an alternative, more robust, and less expensive approach to gather soil information. In this study, a methodology is outlined for mapping spatial distribution of bulk soil average clay content to a depth of 7 m using EM measurements. The study was conducted southeast of Trangie in the lower Macquarie valley of New South Wales, Australia. Two EM sensors were employed. To provide deep bulk soil EM measurements, an EM34 was used in the horizontal dipole mode at coil configurations of 10, 20, and 40 m (respectively, designated EM34-10, EM34-20, and EM34-40). For shallower bulk soil EM measurements, an EM38 was used in vertical and horizontal modes (EM38-v and EM38-h, respectively). A total of 755 locations were measured on a grid of approximately 0.5 km. In order to classify the EM34 data into broad physiographic and hydrogeological units, fuzzy k-means (FKM) classification was applied. By iterating fuzziness exponents (ϕ), input parameters, and evaluating various clustering performance indices, we found optimal classification when $\phi = 1.5$ and number of classes (c) = 4. Fuzzy k-means with extragrade (FKMe) classification was subsequently undertaken to account for Extragrades (i.e., outliers in the data). A spatial response surface sampling (SRSS) design was invoked to select sampling sites within each of the four regular and one Extragrade class. From 40 calibration holes (i.e., 8 from each class), soil samples were taken at 1 m intervals from the soil surface to a depth of 7 m. Each sample was analyzed for clay content then averaged for a 0–7 m clay content (%clay) for each hole. In order to predict the %clay across the landscape, a hierarchical spatial regression model (HSR) was developed using a composite signal variable [i.e.,

* Corresponding author. Tel.: +61 2 9385 8087; fax: +61 2 9385 1558.
  E-mail address: j.triantafilis@unsw.edu.au (J. Triantafilis).

ln(EM34-10) + ln(EM34-40) + ln(EM38-h)] and first-order trend surface components (i.e., Easting and Northing). The final map of %clay generally reflects the known surface clay content and provides information about the spatial distribution of subsurface %clay variability. We conclude that although the FKMe analysis did not result in an improved calibration within each class, the approach delineated similar clusters of signal readings that were useful in providing a framework to determine a soil sampling design that accounted for variations in physiography and hydrogeology.
Published by Elsevier B.V.

1. Introduction

In order to manage the soil resource effectively basic information about its spatial distribution is necessary. One of the most important attributes required by landholders for effective soil use and management is that of clay content. This is particularly the case in the topsoil because (i) it greatly effects the water holding capacity and the hydraulic properties of a soil (Frenkel et al., 1978; Bresler et al., 1984; Jabro, 1992), (ii) it is related to the cation exchange capacity (Russell, 1973), and (iii) it influences the fertility and hence productivity (Davey, 1990). From the hydrological perspective knowledge of the subsoil and vadose zone clay content is also important because large amounts can reduce permeability, inhibit deep drainage, and potentially lead to waterlogged soil conditions (Triantafilis et al., 2003a).

Over the last 30 years various geostatistical and geophysical methods have been employed to enhance the mapping of clay content. Geostatistical methods provide a set of statistical tools for incorporating the spatial coordinates of soil observations in data processing. These methods allow for the description and modeling of spatial patterns, prediction at unsampled locations, and assessment of the uncertainty attached to predictions (Goovaerts, 1999). Various geostatistical approaches have been employed to estimate spatial variation in topsoil clay content. These include, ordinary- (Voltz and Webster, 1990; Kalivas and Kollias, 1999), block- (Mapa and Kumaragamage, 1996), intrinsic random function of order k- (McBratney et al., 1991), indicator- (Oberthur et al., 1999), co- (Vauclin et al., 1983; Zhang et al., 1992), universal- (Odeh et al., 1995), regression- (Odeh and McBratney, 2000), and compositional-kriging (Odeh et al., 2003). Several studies have compared methods (Gallichand and Marcotte, 1993; Odeh et al., 1995) to map subsurface clay.

Soil sampling for geostatistical mapping can be time-consuming and costly. This is particularly the case with respect to identifying and mapping subsurface clay content. In light of this, many studies have incorporated ancillary variables to enhance prediction. The most commonly used method is electromagnetic (EM) induction. EM instruments measure the apparent soil electrical conductivity (EC$_a$), which is a function of various soil properties including salinity, clay content, moisture content, and mineralogy (Triantafilis et al., 2002; Corwin et al., 2003). In the Netherlands, EM survey data have been used to identify the depth to (i) boulder clay (Brus et al., 1992) and (ii) a soft layer in the western marine districts (Knotters et al., 1995). In the USA, EM data have been used to estimate (i) depth to clay pan (Sudduth et al., 1995) and (ii) depositional depth of sand after a large flooding event in the

Midwest of the USA (Kitchen et al., 1996). In Australia, average clay content was mapped using an EM38 at the field level in the lower Gwydir valley (Triantafilis et al., 2001a), while Williams and Hoey (1987) used an EM34 to map average clay content to 7 m.

Despite the improved accuracy and representation of the soil continuum, the methods used to determine sampling locations for calibration are based on subjective judgement that may introduce bias in the final maps. This is best illustrated in the work by Williams and Baker (1982) who found soils of different mineralogy produced different regression relationships between EM34 and soil salinity (as measured in laboratory analysis). What would seem appropriate is the division of the landscape into similar mineralogical or physiographical units prior to site selection, thereby ensuring various parts of the landscape are equally represented in a final calibration model. One approach illustrated by Triantafilis et al. (2003b) used fuzzy *k*-means (FKM) analysis of three channels of EM34 signal data. In effect the method objectively delineated similar physiographical and hydrogeological units in the lower Namoi valley of Australia.

In the following study, we similarly use FKM algorithms (e.g., FKM with extragrades, FKMe) to classify EM34 signal data collected in the lower Macquarie valley. From each of the resulting classes, sampling sites were selected using a model-based spatial response surface sampling (SRSS) design (Lesch, 2005). Our objective was to test the effectiveness of the FKMe classification technique for improving the accuracy of a geostatistical model to predict average clay content (clay%) to a depth of 7 m. A secondary objective was to compare FKMe classes with Pedoderms (i.e., periods in which soil formation takes place) identified by McKenzie (1992) and stratigraphic features of the Trangie district of the lower Macquarie valley in central west New South Wales.

2. Materials and methods

2.1. Study area

The Macquarie River is a tributary of the Darling, which drains the northern part of the Murray–Darling Basin. The study area is located in the lower Macquarie valley southeast of the township of Trangie (Fig. 1). The area includes both irrigated and dryland farms. The latter is mostly wheat (*Triticum aestivum* L.) production and native pastures. Irrigation is mostly for cotton (*Gossypium hirsutum* L.) production. The irrigated infrastructure (including major water reservoirs) of the area is shown in Fig. 1.

McKenzie (1992) identified Pedoderms in the Macquarie valley (Fig. 2). The Trangie Cowal Pedoderm is predominant and is characterized by (i) duplex red-brown profiles (Wilga red-brown) developed from silty parent material, which have a distinct clay maxima between 0.30 and 0.80 m (i.e., 19–35%) and (ii) heavily textured red-brown coloured profiles (Byron) with distinct clay maximum between 0.30 and 0.80 m (i.e., 28–41%). The Old Alluvium Meander Plain Pedoderm is characterized by the Mitchell profile class, which has high coarse sand content that distinguishes it from the other red soil of the alluvial plains. The Old Alluvium Back Plain is more diverse and includes: Mullah—dark grey to black cracking clays (i.e., 51% clay), Snake—sodic grey cracking clays (i.e., 50%) closely related to Mullah, and Buddah profiles characterized by the high clay content (i.e., 48%) of
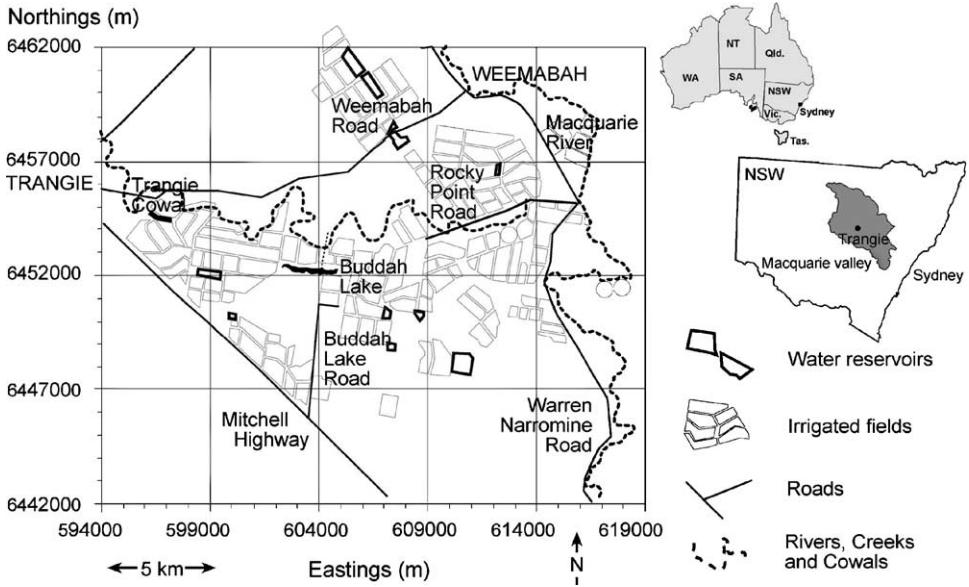
Fig. 1. Location of lower Macquarie valley and major infrastructure in the area southeast of Trangie.
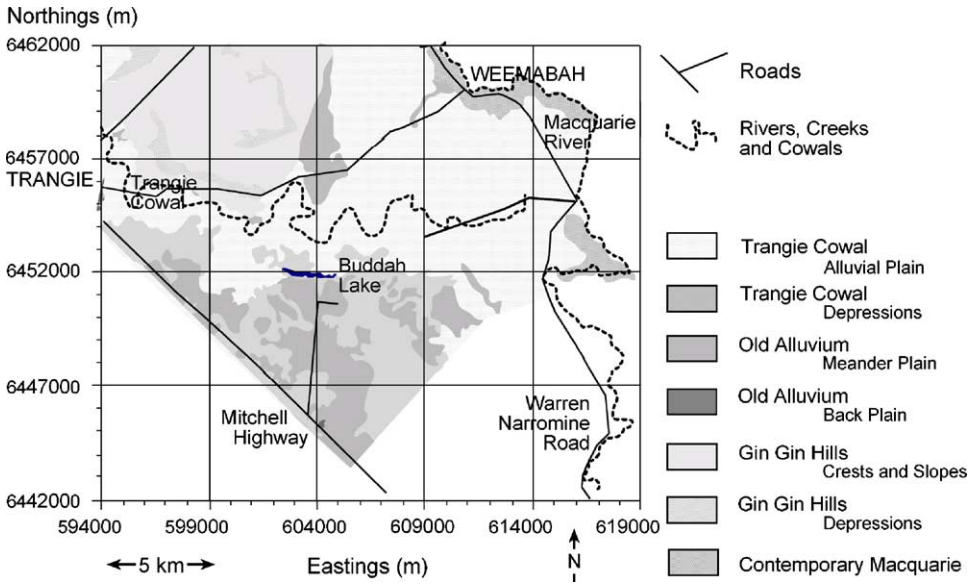

Fig. 2. Pedoderms southeast of Trangie in the Macquarie valley (after McKenzie, 1992).

which smectite and kaolinite clay minerals are co-dominant with illite. The Gin Gin profile class defines the Pedoderm of the same name. The profiles are strongly weathered and have a uniform to gradational texture profile (e.g., 31–40% clay). The Macquarie class, which defines the Macquarie Pedoderm, has minimal profile development and is characterized by considerable fine sand and silt fractions (i.e., median value of 40% at 0.10 m).

2.2. Electromagnetic survey

In order to confirm whether an EM survey could discern these Pedoderms and potentially assist with determining the spatial distribution of vadose-zone clay content and stratigraphic features in the landscape an EM34/38 survey was undertaken across the Trangie study area. Approximately, 500-m grid spacing was used. The first 300 EM34 measurements were obtained in November 1998 and the remaining 455 were recorded in July 2000. At each site, EM34 signal readings were made in the horizontal dipole mode at 10, 20, and 40 m coil configurations (i.e., EM34-10, EM34-20, and EM34-40, respectively). The theoretical depth of measurement is 7.5, 15, and 30 m, respectively (McNeill, 1980). Coordinates were recorded in the Australian Map Grid (AMG84) using a Magellan NavPro5000 GPS. The location of the EM survey positions is shown in Fig. 3. In December of 2001, an EM38 survey was carried out with all 755 sites revisited and measured with the instrument in the vertical (EM38-v) and horizontal (EM38-h) modes of operation. In these modes, the EM38 theoretically measures 1.50 and 0.75 m, respectively (McNeill, 1990).

2.3. Fuzzy k-mean and FKM with extragrades clustering

Various approaches have been developed to enhance information collected at a given site from multiple EM34 measurements. For example, Williams and Arunin (1990) were
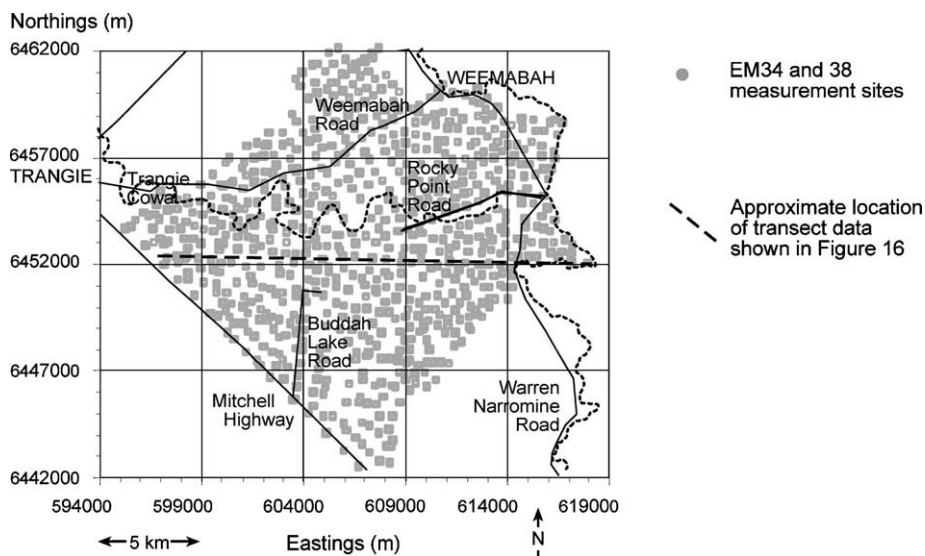

Fig. 3. Location of EM34/38 survey positions southeast of Trangie (Macquarie valley).

able to infer groundwater recharge/discharge areas using what they termed EM Slope (i.e., average ratio of EM34 measurements taken at EM34-10, -20, and -40 m configurations). The results suggested that in a salt-degraded landscape in northeast Thailand, EM Slope values greater or less than 1.0 indicated recharge and discharge areas, respectively. More recently, Triantafilis et al. (2003b) used FKM to objectively classify EM34 signal data collected in the lower Namoi valley of Australia. Using local ordinary kriging (OK) and a method (i.e., log-ratio transformation) that ensures summation of class membership values to unity, they found the final composite fuzzy-class map could be related to the known physiography and geohydrology.

To determine whether equivalent classes could be discerned from FKM analyses of EM34 signal readings (i.e., EM34-10, -20, and -40) collected in the lower Macquarie valley, and possibly identify units of similar vadose-zone properties (i.e., average clay content 0–7 m) we used the method used by Triantafilis et al. (2003b). The FKM approach itself is well described in the literature (McBratney and De Gruijter, 1992; Odeh et al., 1992a; Lagacherie et al., 1997; Triantafilis et al., 2001b). Briefly, the method calculates a measure of the similarity between an individual (i) and a cluster (c), determining how much they are alike in multi-variable space (Bezdek, 1981). The best outcome is the one that minimizes the objective function:

$$J_1(\mathbf{M}, \mathbf{C}) = \sum_{i=1}^{n} \sum_{c=1}^{k} \mu_{ic}^{\phi} d_{ic}^2 \tag{1}$$

where, μ_{ic} is the membership value of the i individual (i.e., EM survey position) and the c cluster. The exponent ϕ determines the degree of fuzziness of the final solution, where the value of $\phi = 1$ is equivalent to the hard partition. The distance dependent metric (d_{ic}^2) is needed to optimize the performance of the objective function (i.e., $J_1(\mathbf{M}, \mathbf{C})$). There are several choices including Euclidean (same scale) and diagonal (different scales), which give equal weight to all measured variables, and Mahalanobis, which is dependent on correlated variables on the same or different scales (McBratney and Moore, 1985).

The FKM algorithms are in accordance with the procedures outlined in Bezdek (1981) and De Gruijter and McBratney (1988). The implementation of $J_1(\mathbf{M}, \mathbf{C})$ was carried out using FuzME2 (Minasny and McBratney, 2002). The validity functionals of fuzziness performance index (FPI) and the normalized classification entropy (NCE) (Roubens, 1982) are used to determine a suitable c and ϕ. The FPI is a measure of the degree of fuzziness while the NCE indicates the degree of disorganization in the classification (Triantafilis et al., 2001b). The least fuzzy and least disorganized number of classes, that is the minimum values, is considered suitable (Odeh et al., 1992a,b). The derivative of $J_1(\mathbf{M}, \mathbf{C})$ versus ϕ can be used to provide a balance between structure and continuity (Bezdek, 1981; McBratney and Moore, 1985):

$$\frac{\mathrm{d}J_1(\mathbf{M}, \mathbf{C})}{\mathrm{d}\phi} = \sum_{i=1}^{n} \sum_{c=1}^{k} \mu_{ic}^{\phi} \log(\mu_{ic}) d_{ic}^2 \tag{2}$$

Ohashi (1984) introduced the concept of a special extragrade class to account for outliers (i.e., individuals that lie outside the main body of data points, which are referred to as

extragrades). As a consequence, the influence of these outliers is reduced and results in compact and more stable classes. De Gruijter and McBratney (1988) developed Eq. (3) so that the memberships directly depend upon the distances to the class centroids:

$$J_2(\mathbf{M}, \mathbf{C}) = \alpha \sum_{i=1}^{n} \sum_{c=1}^{k} \mu_{ic}^{\phi} d_{ic}^2 + (1 - \alpha) \sum_{i=1}^{n} \mu_{i*}^{\phi} \sum_{c=1}^{k} d_{ic}^{-2} \tag{3}$$

The algorithm for solving the equation is found in De Gruijter and McBratney (1988) and is also implemented in the program FuzME2 (Minasny and McBratney, 2002). The program uses Brent's algorithm (Press et al., 1992) for searching an optimal value of *a* rather than the *regula falsi* method as described in De Gruijter and McBratney (1988). The result of FKM clustering is that individual multivariate objects (e.g., a set of EM signal readings) are assigned μ values to each of *c* classes that vary continuously and overlap in attribute space. Centroids for each class are chosen optimally from the data.

2.4. Spatial response surface sampling designs

Sampling designs for collecting and analyzing remotely sensed survey data can be developed using either a design-based or model-based sampling approach. The former are more common, and include simple random sampling, stratified random sampling, multi-stage sampling, cluster sampling, and network sampling schemes, etc. (Thompson, 1992). Model-based designs are less common, although some statistical research has been performed in this area (Valliant et al., 2000). Nathan (1988) and Valliant et al. (2000) discuss the merits of design (probability) and model (prediction)-based sampling strategies in detail. Specific model-based sampling approaches, having direct application to agricultural and environmental survey work, are described by McBratney and Webster (1981), Lesch et al. (1995a,b), Van Groenigen et al. (1999), and Lesch (2005).

The sampling approach discussed in Lesch (2005) and Lesch et al. (1995b) is specifically designed for use with ground-based EM signal readings. In this model-based sampling approach, a minimum set of calibration samples are selected based on the observed magnitudes and spatial locations of the EC_a data, with the explicit goal of optimizing the estimation of a regression model (i.e., minimizing the mean square prediction errors produced by the calibration function). The basis for this sampling approach stems directly from traditional response surface sampling methodology (Box and Draper, 1987). Due to this direct relationship, Lesch et al. (1995b), referred to this site selection process as a "spatial response surface sampling" design.

An SRSS design can be employed to estimate the following empirical regression equation:

$$y_i = b_0 + b_1 S1_i + b_2 S2_i + \ldots + b_k Sk_i + \varepsilon \tag{4}$$

where y_i represents the value of the sample variable at the *i*th site, $S1_i$, $S2_i$, ..., Sk_i represent the *k* sensor readings acquired at this site, b_0, b_1, ..., b_k represent $k + 1$ unknown regression parameters, and ε represents the random error component, which is assumed to exhibit some type of spatial dependence. In the SRSS approach, the goal is to se-

lect a small set of n sample sites ($n \ll N$) that serve to both: (i) optimize the estimation of the regression parameters when using ordinary least squares estimation methods and (ii) minimize the effects of the spatially dependent error structure on this estimation process.

The development of a SRSS design is done via a two-step procedure. In the first step, the errors associated with the hypothetical regression model are assumed to be spatially independent, and the regression equation is viewed as a response surface model. The EM34 signal data is de-correlated using a principal component transformation procedure, and the resulting m principal component vectors are then centered and scaled to have 0 means and unit variance. This principal component data is then directly compared to a suitable response surface design; for example, a factorial design or first- or second-order central composite design composed of n design level combinations balanced across the m principal component vectors (i.e., a design requiring n samples). The n set of principal component scores that most closely match the n response surface design level combinations are then identified and selected as an "optimal" set of sample sites.

In the second step, the residual errors are assumed to be spatially correlated and an iterative adjustment in the sample site locations is attempted. For example, if the model errors follow an isotropic spatial error structure with an effective range ρ, then the algorithm attempts to find substitute sampling locations with minimum separation distances approaching this value. (Note that the assumed spatial error correlation structure approaches independence under these conditions.) In practice, one way this can be achieved is by selecting j distinct sets of "optimal" sample sites (i.e., Step 1 is repeated j times), and then invoking an iterative search routine to identify the best hybrid set of samples out of the n^j possible design level combinations. Lesch (2005) discusses various types of iterative algorithms designed to approximately optimize this spatial arrangement of sample sites in a computationally efficient manner.

2.5. Hierarchical spatial regression models

Two of the most common geostatistical modeling techniques for multivariate spatial data are (i) co-kriging and (ii) kriging with external drift (Wackernagel, 1995; Royle and Berliner, 1999). Both techniques make use of auxiliary data to improve the estimation of a primary variable, although via slightly different modeling assumptions. Co-kriging is generally based on an assumed model for the joint distribution of the variables and can be used to interpolate new predictions of the primary variable anywhere within the sampling domain. In contrast, kriging with external drift (KED) is based on an assumed model for the conditional distribution of the primary variable, given the auxiliary data. Thus, a KED model essentially works like a regression model (where the errors may be spatially correlated), but can only be used to generate predictions where auxiliary data exists.

A hierarchical spatial regression (HSR) model, as introduced by Royle and Berliner (1999), represents an alternate parameterization of a co-kriging model. Like a KED model, a HSR model is based on an assumed model for the conditional distribution of the primary variable, given the auxiliary data. However, the auxiliary data is also assumed to have its own spatial distribution. This hierarchical approach facilitates the predictions of the primary variable anywhere within the sampling domain, similar to a co-kriging model.

It is possible to specify complicated inter-dependence structures in a HSR model; for examples see Royle and Berliner (1999) and Royle et al. (1998). Much more simple, KED-like structures can also be readily specified, such:

$$E(y|z) = \mu_1 + \theta_z + \mathbf{BX} \tag{5.1}$$

$$\text{Var}(y|z) = \mathbf{\Sigma}_1 \tag{5.2}$$

$$E(z) = \mu_2 \tag{5.3}$$

$$\text{Var}(z) = \mathbf{\Sigma}_2 \tag{5.4}$$

where $E(\cdot)$ and $\text{Var}(\cdot)$ represent the expectation and variance of the random variable in question. In this example, y and z represent two spatial variables (i.e., in our case z represents a dense grid of EM signal data and y represents a subset of %clay measurements acquired at a small co-located set of EM signal sites). The first part of the HSR model specifies that y (conditional on observed z data) is linearly related to the co-located z signal level and a linear combination of additional regression parameters (such as trend surface parameters). In standard regression format, $y|z$ might be specified as

$$(y|z = z_0) = \beta_0 + \beta_1[z_0] + \beta_2[x_1] + \beta_3[x_2] + \eta \tag{6}$$

where z_0 represents the observed z signal reading (i.e., EM data), x_1 and x_2 represent scaled location coordinates, β_0 through β_3 represent empirical regression parameters that must be estimated, and η represents the residual error distribution, which may exhibit some type of spatial dependence. In practice, this regression component of the HSR model is estimated using the subset of jointly observed (y, z) data. The second part of the HSR model specifies that z also follows some type of stationary spatial distribution. For example, the covariance function for z might be specified to follow an isotropic exponential model, defined by a set of known hyper-parameters (i.e., nugget, sill, and range parameters). In practice, this covariance function is generally inferred from the observed variogram structure (derived from the entire set of z signal data) and interpolated z-values are normally calculated via an OK analysis. When the conditional error term (η) exhibits spatial dependence, Eq. (6) normally must be estimated using some type of maximum likelihood procedure (Littell et al., 1996). However, when the residual errors can be considered spatially independent, the HSR modeling approach simplifies greatly. Specifically, Eq. (6) can be estimated using ordinary least squares, and then combined with the OK predictions to produce the final interpolated y estimates. The estimate(s) of both the $\hat{y}$ prediction and variance also simplify considerably; i.e.,

(i) at a known (observed) z_0 signal location:

$$\hat{y} = b_0 + b_1(z_0) + b_2(x_1) + b_3(x_2) \tag{7.1}$$

$$\text{Var}(y - \hat{y}) = \sigma^2(1 + \mathbf{u}'(\mathbf{U}'\mathbf{U})^{-1}\mathbf{u}) \tag{7.2}$$

(ii) at an estimated (unobserved) $\hat{z}_u$ signal location:

$$\hat{y} = b_0 + b_1(\hat{z}_u) + b_2(x_1) + b_3(x_2) \tag{8.1}$$

$$\text{Var}(y - \hat{y}) = \sigma^2(1 + \mathbf{v}'(\mathbf{U}'\mathbf{U})^{-1}\mathbf{v}) + b_1^2\text{Var}(\hat{z}_u) \tag{8.2}$$

where u and v represents the current values of the predictor variables, i.e., $\mathbf{u} = (1, z_0, x_1, x_2)$ or $\mathbf{v} = (1, \hat{z}_u, x_1, x_2)$, $\mathbf{U}$ represents the regression model design matrix (based only on the observed spatial predictor data), σ^2 represents the regression model MSE estimate, b_0 through b_3 represents the ordinary least squares regression model parameter estimates, and $\text{Var}(\hat{z}_u)$ represents the kriging variance associated with the $\hat{z}_u$ prediction. Note that Eqs. (8.1) and (8.2) incorporate the prediction and variance results from the OK analysis. A review of OK modeling techniques is given in Wackernagel (1995).

3. Results and discussion

3.1. Exploratory data analysis

Table 1 shows the exploratory data summary statistics pertaining to the 755 EM34 and EM38 signal readings across the Trangie district. Part 1 of Table 1 displays the signal statistics for all five-signal readings, while Parts 2 and 3 show the calculated Pearson cor-

Table 1
EM34 and EM38 summary data statistics

(1) Basic statistics					
Signal	*N*	Mean	Standard deviation	Minimum	Maximum
EM34-10	755	89	38	17	187
EM34-20	755	93	39	10	205
EM34-40	755	115	41	28	223
EM-38v	755	88	44	5	256
EM-38h	755	75	34	13	204

(2) Pearson correlation coefficients: raw signal data					
Signal	EM34-10	EM34-20	EM34-40	EM38-v	EM38-h
EM34-10	1.00	0.89	0.75	0.77	0.69
EM34-20		1.00	0.87	0.68	0.60
EM34-40			1.00	0.56	0.49
EM-38v				1.00	0.94
EM-38h					1.00

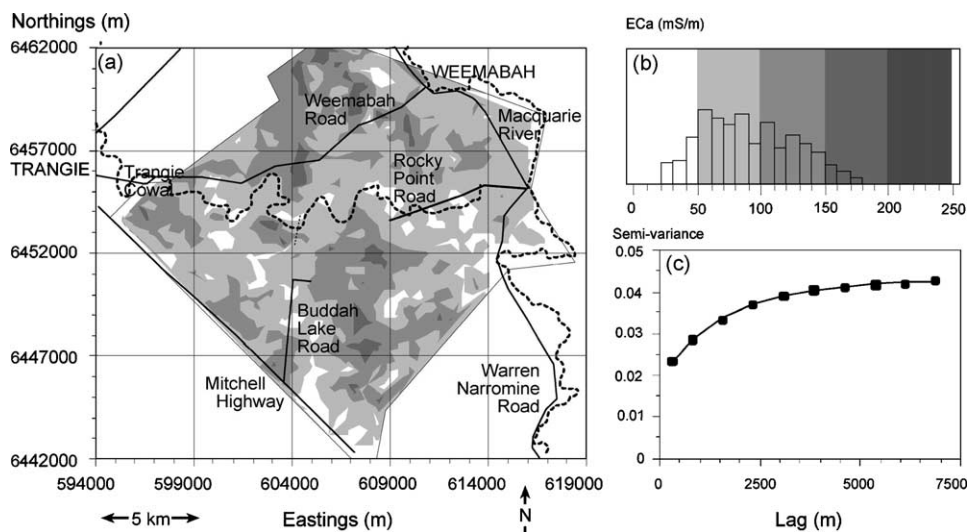| (3) Pearson correlation coefficients: natural log (ln)transformed signal data					
Signal	EM34-10	EM34-20	EM34-40	EM38-v	EM38-h
EM34-10	1.00	0.89	0.75	0.75	0.71
EM34-20		1.00	0.86	0.66	0.60
EM34-40			1.00	0.55	0.50
EM-38v				1.00	0.94
EM-38h					1.00

Fig. 4. EM34 signal data (mS/m) in the horizontal dipole and 10 m (EM34-10) configuration: (a) contour plot, (b) frequency distribution, and (c) calculated variogram structure and exponential model.

relation matrices for the raw and natural log (ln)-transformed signal data, respectively. The EM34 tended to produce signal readings that were slightly higher than the corresponding EM38, although both instruments displayed a similar range. The highest average signal readings were recorded by the EM34-40 (115 mS/m), while the lowest average readings were recorded by the EM38-h (75 mS/m). Overall, the EM38-v exhibited the highest standard deviation (44 mS/m) and the largest range (5–256 mS/m). The histograms of all five-signal readings were slightly right-skewed (e.g., Figs. 4b–6b), and all five distributions failed the Shapiro–Wilk Normality test (Shapiro and Wilk, 1965) at the 0.0001 significance level.

The Pearson correlation matrices shown in Table 1 (Part 2) indicate that all five-signal readings are strongly correlated with each other. Asymptotic χ^2-tests confirm that this observed correlation structure is significantly different from both the Identity matrix and an intra-class correlation structure ($p < 0.0001$). The highest correlation estimate observed in the ln-transformed matrix occurs between the EM38-h and EM38-v signal readings ($r = 0.94$). The next highest estimates tend to be associated with the various EM34 signal vectors. The EM34 and EM38 cross-correlation estimates generally appear to be the lowest, but still range from 0.50 to 0.75. The calculated isotropic variograms for some of the signal vectors are shown in Figs. 4c–6c. Each variogram plot suggests that the corresponding signal data exhibits strong spatial correlation, but also significant local discontinuity (as indicated by the apparently large nugget components).

3.2. Spatial distribution of EC_a

Fig. 4 shows the spatial distribution of EM34-10. The coarser sediments of the Trangie Cowal, which runs east to west through the midline of the study area, is characterized by
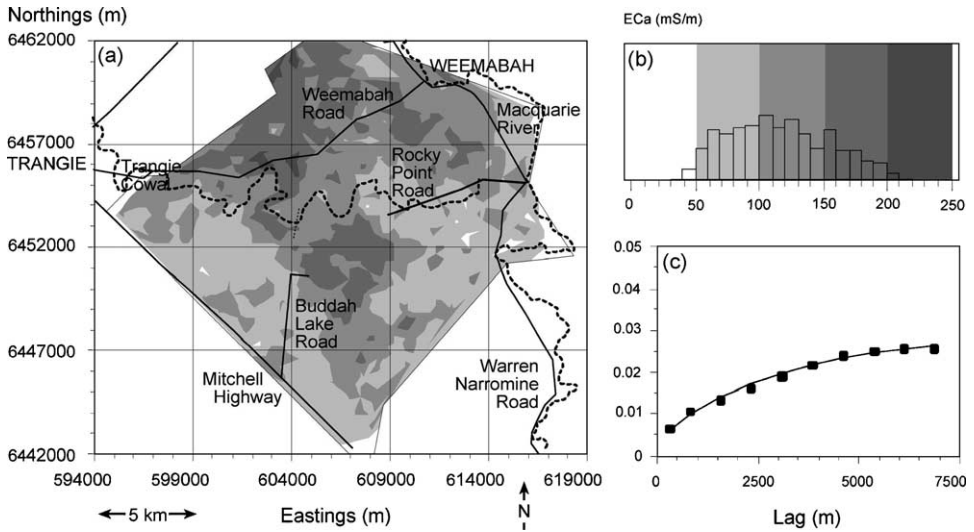
Fig. 5. EM34 signal data (mS/m) in the horizontal dipole and 40 m (EM34-40) configuration: (a) contour plot, (b) frequency distribution, and (c) calculated variogram structure and exponential model.

low readings (i.e., <100 mS/m). This is also the case for the Old Alluvium (Meander Plain), located in the western part of the study area and running parallel to the Mitchell Highway. The lowest signal readings (i.e., <50 mS/m) were associated with the Contemporary Macquarie Pedoderm adjacent to the modern-day Macquarie River. Above average signal
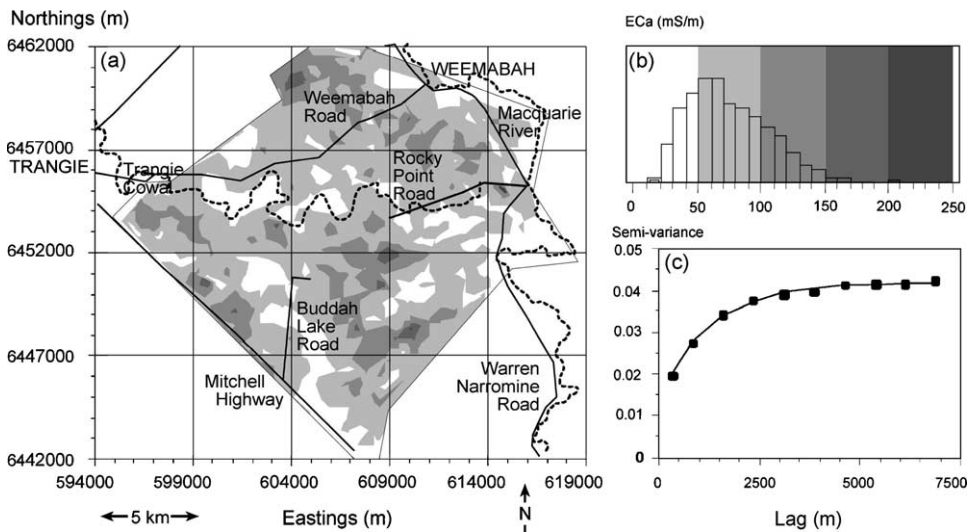

Fig. 6. EM38 signal data (mS/m) in the horizontal dipole (EM38-h) configuration: (a) contour plot, (b) frequency distribution, and (c) calculated variogram structure and exponential model.

readings (i.e., 100–150 mS/m) were recorded south of the Trangie Cowal near Trangie and to the east and west of Buddah Lake Road. Here, the soil is associated with the clayier sediments of the Old Alluvium (Back Plain) along the western margin of the area. Towards the Macquarie River and to the north and south of the Weemabah Road signal readings were similarly high in areas associated with the Trangie Cowal Depressions and Alluvial Plain. The EC_a pattern obtained with the EM34-20 m was similar (figure not shown).

Fig. 5 shows the contour plot of signal readings recorded with the EM34-40. Despite the fact EC_a signal readings were generally higher than the EM34-10 readings, the spatial patterns of the two were similar, with the lowest readings (i.e., <100 mS/m) associated with the Old Alluvium (Meander Plain) and areas directly adjacent to the Trangie Cowal and contemporary Macquarie River. Intermediate to higher signal readings (i.e., >100 mS/m) were associated with the Old Alluvium (Back Plain) in the central southern part of the area and north of the Weemabah Road underlying the sediments of the Gin Gin Hills and Trangie Cowal (i.e., Depressions) Pedoderms. This was similarly the case between the Weemabah and Rocky Point Roads, underlying the Trangie Cowal Alluvial Plains. The higher readings recorded are consistent with a known saline aquifer that occurs within 13–15 m of the ground surface in these locals.

Fig. 6 shows the pattern of signal readings obtained with the EM38-h. It is evident that the readings collected in the root zone (i.e., 0–0.75 m) are generally less than 100 mS/m and that the spatial pattern is similar to that achieved using the EM34-10 (see Fig. 4a). The major difference in the signal reading is that apart from a few locals, the Trangie Cowal (Alluvial Plains) Pedoderm is characterized by signal readings of less than 100 mS/m. To the north of Weemabah Road, the larger readings are associated with clayier soil types. However, to the south the higher readings are due in some part to the isolated point source salinization evident in parts of this property. The pattern obtained with the EM38-v was similar to that shown in Fig. 6a.

3.3. FKM and FKMe analysis

In view of the high correlation between the various EM34 signal readings (Table 1), we used Mahalanobis as the distance metric as it accounts for the differences in variances and correlations among variables (Bezdek, 1981). At the time of carrying out the FKM analysis the EM38 data was not available. In deciding the number of classes, we examined the outcomes of $J_1(\mathbf{M}, \mathbf{C})$ partitioning of the three signal readings of the EM34 into $c = 2$–8 using $\phi = 1.1, 1.3, 1.5, 1.7$, and 1.9. Fig. 7a and b suggest that the best solution was probably $c = 4, 5$, or 6 because both the FPI and NCE were a minimum here. The results of ϕ versus $-(dJ_1(\mathbf{M}, \mathbf{C})/d\phi)c^{0.5}$ is shown in Fig. 8. McBratney and Moore (1985) suggested that the highest class value of $-(dJ_1(\mathbf{M}, \mathbf{C})/d\phi)c^{0.5}$ can be considered optimal. In this case, it was $\phi = 1.5$ for $c = 4$–6 classes. On reviewing Fig. 7a, we conclude that FPI is a minimum when $c = 4$ and when $\phi = 1.5$. In order to account for individuals which do not fit in these four classes, we re-classified the data using $J_2(\mathbf{M}, \mathbf{C})$, so that these individuals would be accounted for by an Extragrade class.

Table 2 shows a portion of the FKMe membership matrix for $c = 4$ (i.e., A, B, C, D) regular and the Extragrade class using $\phi = 1.5$. Because membership sums to unity, this type of data is referred to as closed or compositional data (Aitchison, 1986). As Pawlowsky
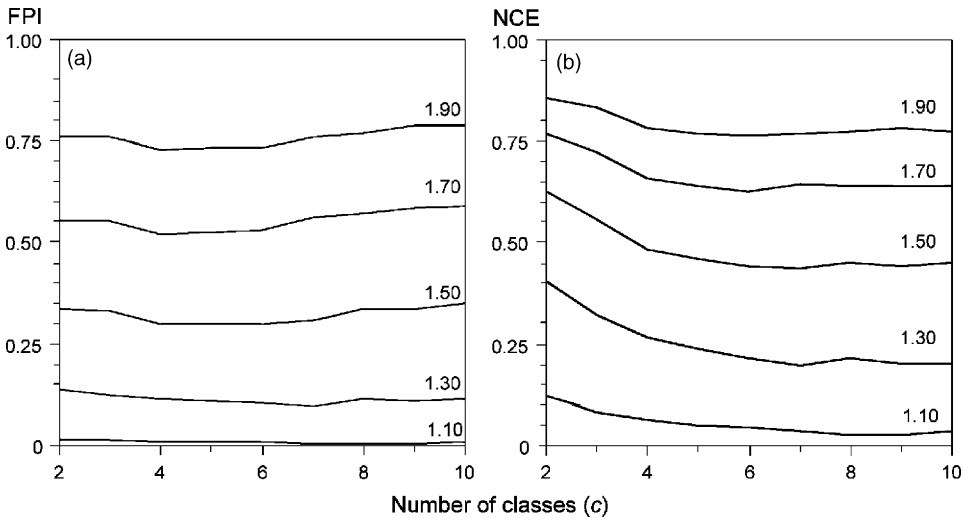
Fig. 7. Validity functionals (a) fuzziness performance index (FPI) and (b) normalized classification entropy (NCE) vs. number of classes (c) for fuzziness exponents (ϕ) = 1.10–1.90.

(1984) points out regionalized compositions are characterized by components that can be modeled by a spatial random function, are positive definite and sum to a constant. When interpolating compositional data, the method used should satisfy these criteria (Odeh et al., 2003). Walvoort and De Gruijter (2001) introduced the method of compositional kriging that complies with these constraints and is basically an extension of OK. Another approach is the use of additive log-ratio (ALR) transformation (McBratney et al., 1992),
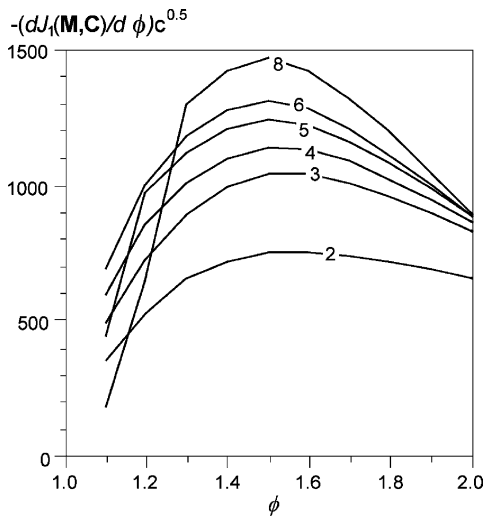

Fig. 8. Plot of fuzziness exponent (ϕ) vs. $-[(dJ_1(\mathbf{M},\mathbf{C})/d\phi)c^{0.5}]$ for classes (c) = 2, ..., 8.

Table 2
A small portion of the fuzzy k-means with Extragrades (FKMe) membership matrix for classes $(c) = 4$ and an Extragrade class using a fuzziness exponent $(\phi) = 1.5$

Site ID	Class A	Class B	Class C	Class D	Extragrades
1	0.034	0.954	0.002	0.008	0.002
2	0.159	0.696	0.013	0.028	0.103
3	0.040	0.875	0.006	0.024	0.055
4	0.048	0.867	0.007	0.024	0.055
5	0.004	0.993	0.000	0.003	0.000
.	.	.	.	.	.
.	.	.	.	.	.
.	.	.	.	.	.
755	0.120	0.075	0.149	0.642	0.015

which briefly involves OK log-ratio-transformed membership values with a non-linear back transformation.

Fig. 9 shows the composite fuzzy class map for $c = 4$ regular and the Extragrade class when $\phi = 1.5$ using the ALR method. The map shows the union of membership (μ) values exceeding 0.5. The white areas represent the intergrades, where membership was less than 0.5. Classes A and B represent the least conductive parts of the landscape. Class A represented the second lowest signal readings using the EM34-10 and EM34-20 m configurations. However, at the 40 m configuration, the readings were on average second highest. With respect to the Trangie Cowal in the west, this is consistent with the areas where the surface expression of soil salinity is apparent (i.e., saline water tables occur near large earthen
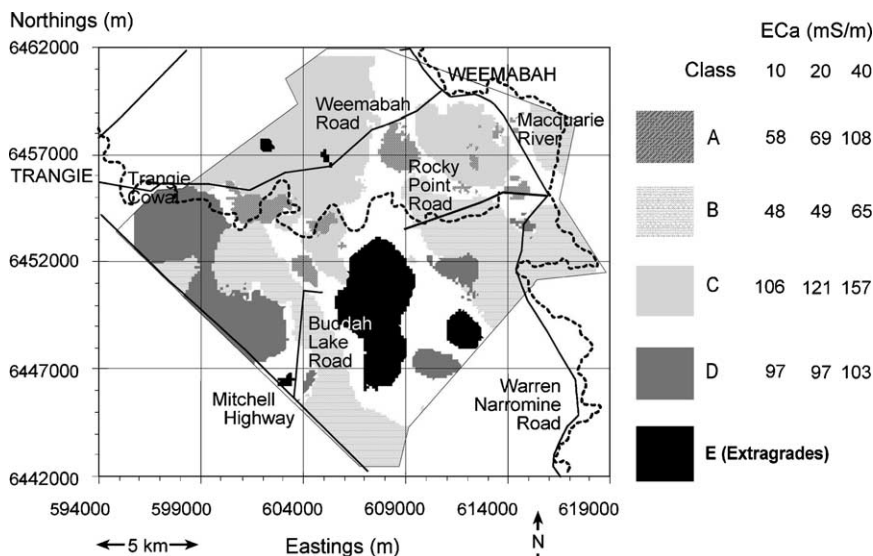

Fig. 9. Map of composite fuzzy classes for $(c) = 4$ (i.e., Classes A, B, C, and D) plus the Extragrade class when fuzziness exponent (ϕ) is 1.5. *Note:* Centroid values (EM34 signal readings in mS/m) are shown for each class.

storages and supply channels between Weemabah and Rocky Point Roads). Class A had the smallest number of members (i.e., 113) and as a consequence of being spread out evenly across the district, the class was not readily mappable. Where it appeared in contiguous numbers, the class was associated with the Trangie Cowal (Alluvial Plain) Pedoderm. Class B had the lowest signal readings across all EM34 configurations and represented the coarse sediments of the Trangie Cowal and Old Alluvium (Meander Plain) Pedoderms. It had the largest number of spatially contiguous members (i.e., 173). Two areas were evident. The first is associated with the Trangie Cowal (Alluvial Plain) and the Contemporary Macquarie Pedoderms. The second area coincides with the Old Alluvium (Meander Plain) Pedoderm in the west.

Classes C and D represented the more conductive parts of the Trangie district. Class C has the second lowest membership (i.e., 124) but is defined by the greatest signal readings, which progressively increase with depth. The largest contiguous area mapped is located in the central northern part of the study area, associated with the Gin Gin Hills (Crests and Slopes, and Depressions) and Trangie Cowal (Alluvial Plain and Depressions) Pedoderms. In these areas, saline aquifers and water tables are known to exist. Class D had the second largest number of members (i.e., 161). The class is characterized by uniformly conductive readings (i.e., 97, 97, and 103 mS/m for EM34-10, -20, and -40, respectively). Most members were associated with the Old Alluvium (Back Plain) south of the Township of Trangie. A total of 139 sites were classed as Extragrades. Most of these were found in a large cluster associated with the Old Alluvium (Back Plain) Pedoderm in the central southern part of the study area.

In order to identify where there is overlap or uncertainty in the composite fuzzy class map shown in Fig. 9 we calculated and mapped the confusion index (CI). The method is described in Burrough et al. (1997) and was developed to assist in identifying where more information may be appropriate in order to better understand the nature of the overlap between classes. Fig. 10 shows the map of CI when $c = 4 + 1$ Extragrade classes. The white areas (CI ≤ 0.2) indicate where there is little uncertainty in the classification. It is evident that of all the classes, the area defined by Class B has the least uncertainty associated with it. Conversely, the darker shaded areas indicate where the CI > 0.6 (i.e., intragrades) and therefore where uncertainty is greatest. It is evident that the largest contiguous area of uncertainty (CI > 0.4) coincides with the central part of the district to the north of the area delineated by the Extragrade class and between Classes C and B.

There are two possible explanations as to why the large uncertainty in the classification, in this local, is attributable to land use. In the first instance, the area coincides with a small pocket of dryland agriculture, which is surrounded on two sides by intensively irrigated farms. As Vaughan et al. (1995) point out, the effect of management practices (i.e., dryland and irrigated fields) can significantly influence the moisture content of the soil and hence potentially measurements made with EM instruments at the district level. This is particularly the case for instruments or configurations that measure the near surface (i.e., EM38). Secondly, and perhaps more significantly, the area of higher uncertainty lies to the east of where the Trangie Cowal (Alluvial Plain) Pedoderm narrows between the Old Alluvium (Back Plain) north of Buddah Lake and the Gin Gin Hills Pedoderm (see Fig. 2). The significance of this is that these Pedoderms contain surface sediments that are clayier than those associated with the Trangie Cowal. If these sediments extend to depth, this may produce
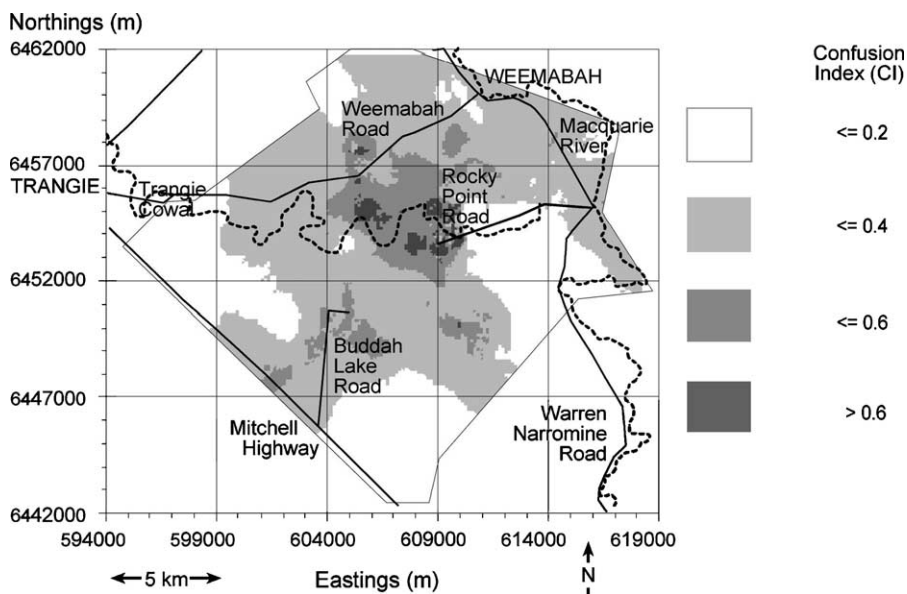
Fig. 10. Map of confusion index (CI) for classes (c) = 4 (i.e., Classes A, B, C, and D) plus the Extragrade class when fuzziness exponent (ϕ) is 1.5.

a geohydrological constriction, which will result in water flow being impeded to the west. This perhaps explains the presence of saline water tables adjacent to the western most fields of the landholding north of Rocky Point Road.

3.4. Combining FKMe clustering with a SRSS design

From a statistical perspective, the FKMe analysis essentially imposed a "blocking" structure over the full data set. In turn, this implied that the final, composite SRSS design had to be compiled together from smaller, individual SRSS designs generated on each fuzzy class (i.e., Classes A, B, C, D, and one Extragrade class). Therefore, a composite SRSS design was generated from the EM34 survey data. First, individual SRSS designs were independently generated within each fuzzy class. Since the EM34 survey data consisted of three signal readings per site (i.e., EM34-10, -20, and -40 m configurations), a 2^3 factorial response surface design was used to generate 8 sampling locations in each sub-region. The factorial design levels in all designs were set at ±1.5, which corresponded to a shift of 1.5 standard deviations above or below the mean level of each principal component vector. The effective range of the residual error correlation structure was assumed to be arbitrarily large, and hence the algorithm selected the maximum potential separation distances. Next, after an initial SRSS design was generated in each of the fuzzy classes, two additional independent SRSS designs were generated in each of the four regular classes (i.e., c = A, B, C, and D) and the Extragrade class. This resulted in a total of 15 individual SRSS designs across the five classes.
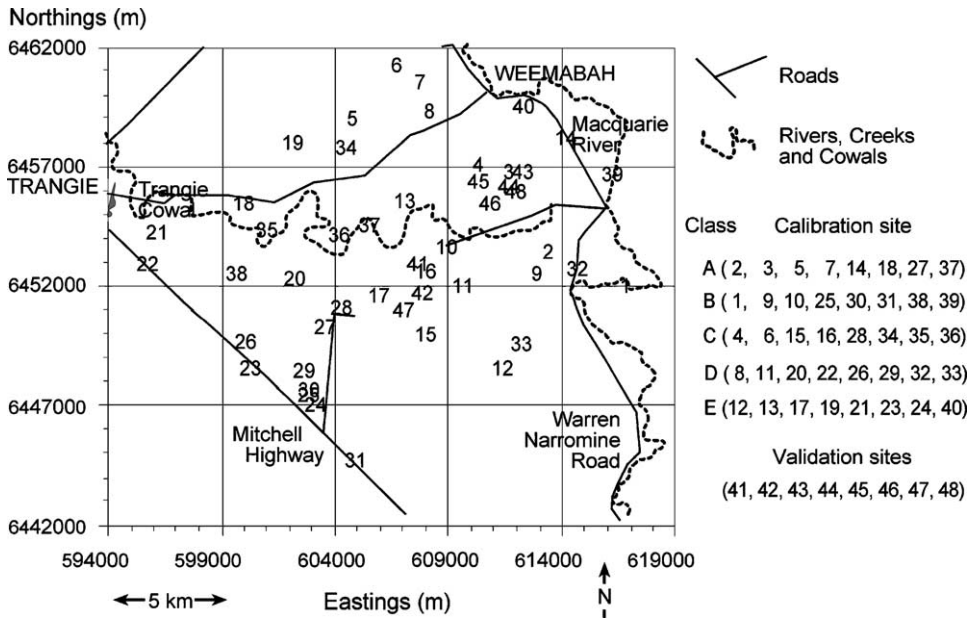
Fig. 11. Location of 40 soil sampling sites + 8 validation sites.

Any given design within a class could have been selected as the target design for that class without any significant loss in prediction efficiency. However, the reason for the generation of multiple designs was that a large number of potential composite SRSS designs could be assembled and analyzed for their overall spatial uniformity. Specifically, there were a total of $3^5 = 243$ possible ways to construct the composite design across the five fuzzy-set classes. The final composite sampling plan was formed by sequentially generating all 243 potential composite designs. The combination (of individual designs) that produced the maximum spatial uniformity (i.e., greatest average separation between sample sites) across the entire survey region was selected. Note that this optimization criteria was used in order to minimize the possibility of spatial dependence in the residual error distribution.

Fig. 11 shows the locations of the final 40 sample site locations chosen by the composite SRSS design, with respect to the entire 755 EM survey sites. The average minimum separation distance achieved by this design was approximately 1000 m. In addition, Fig. 11 shows the location of eight validation sites. At each calibration site a soil sample was taken every 1 m from the soil surface to a depth of 7 m. The particle size fraction was determined on each sample using the hydrometer method (Rayment and Higginson, 1992). An average clay content value to a depth of 7 m (i.e., %clay) was then determined at each calibration and validation site.

3.5. Relationship between EC_a and average soil clay content to 7 m (%clay)

Table 3 shows the corresponding data summary statistics pertaining to the EM34 and EM38 signal readings and %clay calibration data collected at the 40 sample sites within the

Table 3

EM34 and EM38 versus average clay content to 7 m (%clay) calibration sample data: basic summary statistics and correlation estimates

(1) Basic statistics

Variable	N	Mean	Standard deviation	Minimum	Maximum
%clay	40	41	10	15	58
EM34-10	40	90	41	21	162
EM34-20	40	102	44	29	192
EM34-40	40	114	46	28	203
EM38-v	40	83	45	5	159
EM38-h	40	77	40	13	147

(2) Pearson correlation coefficients: ln-transformed signal data vs. %clay

Signal	r^2
ln EM34-10	0.83
ln EM34-20	0.77
ln EM34-40	0.66
ln EM38-v	0.81
ln EM38-h	0.82

study area. Part 1 of Table 3 shows the basic statistics associated with these calibration data, while Part 2 shows the calculated correlation estimates between the %clay and each EM signal reading. The %clay measurements ranged from 15 to 58%, with a mean value of 41% and a standard deviation of 10%. A histogram of the %clay data revealed a distribution that appeared to be slightly left-skewed (figure not shown), but not especially asymmetrical. The mean EM34 (and EM38) signal readings across the 40 calibration sites were quite close to the global means (shown in Table 1), and the calculated standard deviations were slightly higher. These results were expected, since the composite SRSS sampling approach (used to select the 40 sites) is specifically designed to cover the full signal range while preserving the data "balance" (i.e., this sampling approach constrains the sample means to be approximately the same as the global means). The Pearson correlation coefficients between each ln-transformed EM signal and the %clay ranged from 0.66 to 0.83; all five correlation estimates are statistically significant below the 0.0001 level.

3.6. Testing the usefulness of the FKMe classes

The FKMe selection strategy identified five distinct subsets (i.e., Classes A, B, C, D, and the Extragrade class) of EM34 data observations. These classes identified different EM34 data response patterns, and thus supposedly identify distinct sub-regions where the response variable would be expected to be different. Table 4 shows the average %clay estimates associated with each class. Both the mean levels and corresponding standard deviations appear to be somewhat different. One-way analysis of variance (ANOVA) F-tests suggest that these differences are significant below the 0.1 level (common variance assumption: $F = 3.08$, $p = 0.028$; unequal variance assumption: $F = 2.37$, $p = 0.071$; Levene test for the common variance assumption: $F = 2.61$, $p = 0.052$). These results are not especially surprising, given the strong correlation between %clay and the EM34 signal

Table 4
Average clay content to 7 m (%clay) summary statistics associated with each fuzzy k-mean class

Basic %clay statistics (by fuzzy k-mean class)						
Class	N	Mean	Standard deviation	Standard error	Minimum	Maximum
A	8	32.8	12.6	4.4	15.0	44.0
B	8	37.1	9.5	3.4	23.1	51.5
C	8	45.5	8.4	3.0	31.8	58.0
D	8	43.8	5.6	2.0	35.2	50.2
Extragrades	8	44.6	7.1	2.5	28.9	50.9

data. The FKMe procedure essentially stratified the EM34 signal data into classes with different mean signal levels, etc. However, a more important question is whether the apparent %clay versus EM relationship changes across classes.

To address this question statistically, the following multiple linear regression model was first fit to the full %clay versus EM34 calibration data set:

Model 1 (Base model):

$$\text{\%clay} = \beta_0 + \beta_1(w_{10}) + \beta_2(w_{20}) + \beta_3(w_{40}) + \beta_4(X_s) + \beta_5(Y_s) + \varepsilon \tag{9}$$

where $w_{10} = \ln(\text{EM34-10})$, $w_{20} = \ln(\text{EM34-20})$, $w_{40} = \ln(\text{EM34-40})$, $X_s = (\text{Easting} - 600,000)/10,000$, $Y_s = (\text{Northing} - 6,440,000)/10,000$, and β_0 through β_5 represent empirical regression model parameters.

Model 1 specifies an additive linear relationship between the %clay and ln-transformed EM34 signal data (w_{10}, w_{20}, w_{40}), and also adjusts for linear drift in the predicted response using first-order trend surface components (X_s, Y_s). No EM38 data is used in this model, since the original FKM classification procedure was based solely on the three EM34 signal vectors. However, trend surface parameters (β_4, β_5) were added to this base model to account for a noticeable north–south linear drift in the (non-trend surface adjusted) residual error pattern. The regression model summary statistics and parameter estimates for this model are given in Table 5. After this base model had been specified, the following two additional analysis of covariance (ANOCOVA) models were fit to the same %clay versus EM34 calibration data set:

Table 5
Regression model summary statistics for EM34 base model (Eq. (9))

(1) Model summary statistics	
RMSE	5.06
r^2	0.77

(2) Parameter estimates				
Variable	Parameter estimate	Standard error	t-test	$p > |t|$
Intercept	−17.54	8.39	−2.09	0.044
ln EM34-10	11.63	4.45	2.61	0.013
ln EM34-20	0.24	6.25	0.04	0.969
ln EM34-40	3.41	4.21	0.81	0.422
X_s (scaled X)	0.96	1.61	0.60	0.556
Y_s (scaled Y)	−7.46	2.24	−3.33	0.002

Model 2 (Variable Intercept model):

$$\%\text{clay} = \beta_0 + \alpha_j(\text{Fc}) + \beta_1(w_{10}) + \beta_2(w_{20}) + \beta_3(w_{40}) + \beta_4(X_s) + \beta_5(Y_s) + \varepsilon$$

$$(10)$$

Model 3 (Variable Intercept and Slope model):

$$\%\text{clay} = \beta_0 + \alpha_j(\text{Fc}) + \delta_{j1}(w_{10}) + \delta_{j2}(w_{20}) + \delta_{j3}(w_{40}) + \beta_4(X_s) + \beta_5(Y_s) + \varepsilon$$

$$(11)$$

where Fc represents the fuzzy class (e.g., Class A) and α_j, δ_{j1}, δ_{j2}, and δ_{j3} represent additional empirical model parameters. Model 2 includes the fuzzy class blocking effect, in addition to all of the base model (Model 1) parameters. Thus, Model 2 represents an expanded version of Model 1, where now each fuzzy class is allowed to have a different intercept parameter estimate. Model 3 represents a more complex version of Model 2; in this latter model the entire linear relationship [between the %clay and ln(EM34) data] can change across each fuzzy class.

Models 2 and 3 were then each tested against Model 1 using a General *F*-testing approach (Weisberg, 1985). These two general *F*-tests corresponded to the following parameter tests:

1. Model 2 versus Model 1
   $$\alpha_j = 0, \quad \text{for all } j$$
2. Model 3 versus Model 1
   $$\alpha_j = 0, \ \delta_{j1} = \beta_1, \ \delta_{j2} = \beta_2, \ \delta_{j2} = \beta_3, \quad \text{for all } j$$

Neither the first ($F = 0.821$, $p = 0.522$) nor second ($F = 1.691$, $p = 0.142$) test results were statistically significant. These results suggest that the functional form of the regression model does not significantly change across the five fuzzy classes. In other words, the base model (Model 1) provides the most parsimonious description of the %clay versus ln(EM34) signal data relationship. Based on these test results, it appears that the additional sampling stratification (imposed by the FKM algorithm) cannot be used to increase the precision of the prediction model. A homogeneous regression model appears to be adequate, regardless of which fuzzy class the EM34 signal data originates from.

3.7. Estimation of the regression equation (used in the HSR Model)

Table 6 shows the revised model summary statistics and parameter estimates for the expanded version of Model 1 that conditions on both EM34 and EM38 signal data. Although the r^2-value is higher (0.79) and the root mean square error (RMSE) estimate is lower (4.95) for this model (compared to the EM34 only model), none of the individual EM signal parameter estimates appear to be statistically significant. This apparent lack of significance is actually due to the fairly high correlation (co-linearity) between the various ln EM signal vectors, and suggests that a reduced set of prediction vectors should be used instead.

We employed a forward sequential variable selection procedure to help select an optimal reduced set of signal parameters (Myers, 1986). In this procedure, the two trend surface parameters were forced into the model; the remaining five signal parameters were sequentially

Table 6

Regression model summary statistics for full EM34 and EM38 model

(1) Model summary statistics

RMSE	4.947
r^2	0.793

(2) Parameter estimates

Variable	Parameter estimate	Standard error	t-test	$p > |t|$
Intercept	−16.56	8.92	−1.86	0.073
ln EM34-10	5.48	5.42	1.01	0.320
ln EM34-20	−1.23	6.21	−0.20	0.845
ln EM34-40	5.87	4.37	1.34	0.188
ln EM38-v	1.68	3.51	0.48	0.636
ln EM38-h	3.20	4.54	0.71	0.486
X_s (scaled X)	0.59	1.59	0.37	0.713
Y_s (scaled Y)	−6.70	2.25	−2.98	0.006

entered if and only if they resulted in a significance level of <0.25 (SAS: Reg procedure, 1990). This forward selection procedure identified the ln-transformed EM34-10 and EM34-40 and EM38-h signal data vectors for inclusion into the model. Additional stepwise and backwards selection procedures also identified these same three data vectors. The regression model summary statistics and parameter estimates for this model are given in Table 7. The forward variable selection procedure successfully identified a more parsimonious parameter structure, as demonstrated by the slightly reduced MSE estimate (4.82). However, the parameter estimates shown also suggest that all three signal parameter values (5.16, 5.36, and 4.86) are probably equivalent. An F-test of $\beta_1 = \beta_2 = \beta_3$ confirms this ($F = 0.02$, $p = 0.99$), and implies that the individual ln(EM34-10), ln(EM34-40), and ln(EM38-h) signal vectors should be combined together into a single, composite predictor variable.

Given these results, we defined a new composite signal variable (c-ln EM) as c-ln EM = [ln(EM34-10) + ln(EM34-40) + ln(EM38-h)] and then estimated the following lin-

Table 7

Regression model summary statistics for the reduced EM34 and EM38 model derived using the forward modeling procedure

(1) Model summary statistics

RMSE	4.821
r^2	0.791

(2) Parameter estimates

Variable	Parameter estimate	Standard error	t-test	$p > |t|$
Intercept	−18.21	7.99	−2.28	0.029
ln EM34-10	5.16	4.38	1.18	0.247
ln EM34-40	5.36	3.22	1.66	0.106
ln EM38-h	4.86	2.59	1.88	0.069
X_s (scaled X)	0.57	1.54	0.37	0.715
Y_s (scaled Y)	−6.66	2.17	−3.07	0.004

Table 8

Regression model summary statistics for the final electromagnetic (EM) model using the composite signal variable c-ln EM (Eq. (12))

(1) Model summary statistics				
RMSE				4.687
r^2				0.791

(2) Parameter estimates				
Variable	Parameter estimate	Standard error	t-test	$p > |t|$
Intercept	−17.78	7.18	−2.48	0.018
c-ln EM	5.09	0.48	10.54	0.000
X_s (scaled X)	0.55	1.47	0.37	0.711
Y_s (scaled Y)	−6.52	1.89	−3.45	0.001

ear regression model:

$$\%\text{clay} = \beta_0 + \beta_1(\text{c-lnEM}) + \beta_2(X_s) + \beta_3(Y_s) + \varepsilon \tag{12}$$

The regression model summary statistics and parameter estimates for this model are given in Table 8. With respect to the model produced by the forward variable selection procedure, the r^2-value remained unchanged (0.79) and the new MSE estimate (4.69) was slightly reduced. A plot of the predicted versus observed %clay measurements across the 40 calibration sites is shown in Fig. 12.

A complete residual analysis was performed to assess the adequacy of the final %clay prediction model. This analysis included examining the error structure for outliers and/or highly influential observations, testing the residual error distribution for normality, and testing for spatial correlation in the residual error pattern using a modified Moran residual test statistic (Brandsma and Ketellapper, 1979). Some summary statistics pertaining to
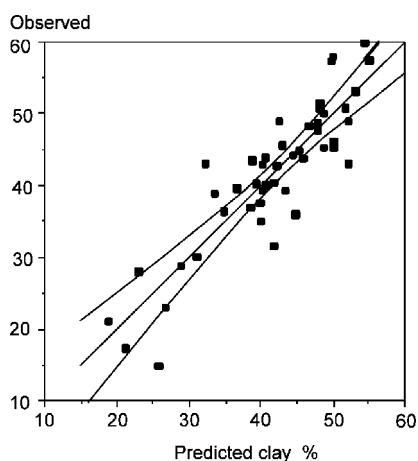

Fig. 12. Observed vs. regression model predicted average clay content to 7 m (%clay) measurements [using Eq. (12)].

Table 9
Residual diagnostic and test statistics associated with the final electromagnetic (EM) model (Eq. (12))

(1) Univariate residual summary statistics	Mean	Standard deviation	Minimum	Maximum
Residuals	0.00	4.50	-10.95	9.91
Student residuals	−0.01	1.05	-2.80	2.37
(2) Maximum observed HAT leverage value	0.2071			
(3) Shapiro–Wilk test statistic (test for normality)				
W	0.9784			
$p < W$	0.6318			
(4) Modified Moran test-statistic (test for spatial correlation)				
Im-score	−0.070			
$E[Im]$	−0.063			
$Var[Im]$	0.006			
z-score	−0.10			
$p > z$	0.540			

this analysis are presented in Table 9. The residual error pattern revealed no outliers or highly influential observations. Additionally, the error distribution passed the Shapiro–Wilk Normality test ($W = 0.9784$, $p = 0.6318$) and the modified Moran spatial correlation test ($z = -0.10$, $p = 0.540$). These results suggest that the assumptions of residual normality and spatial independence are valid for this regression model.

3.8. Estimating the spatial covariance structure of the composite signal data

As explained previously, the estimation of a HSR model is a two-step process. The first step involves the estimation of a suitable regression model describing the response versus predictor relationship, conditioned on any fixed trend surface and/or blocking parameters and the known (i.e., observed) spatial predictors. The second step involves the determination of the spatial covariance structure of the spatial predictor(s). In Eq. (12), there is only one spatial predictor (the c-ln EM signal term) and hence only one spatial variance structure needed to be estimated. Fig. 13 shows the isotropic variogram calculated from the c-ln EM data, with an exponential variogram model superimposed. A second-order stationary, isotropic exponential model produced the most parsimonious fit to the observed variogram structure (no apparent anisotropic structure was detected). The nugget (σ_n^2), total sill ($\sigma_n^2 + \sigma_s^2$), and range (υ) parameter estimates for this model were calculated to be 0.51, 1.48, and 2120 m, respectively. Note that this fitted variogram model corresponds to the following c-ln EM spatial covariance structure:

$$C(h) = \begin{cases} 1.48, & |h| = 0 \\ 0.51 \ \exp\left(-\frac{3|h|}{2120}\right), & |h| > 0 \end{cases}$$

A cross-validation kriging analysis using this covariance model yielded an approximately 1:1 set of predictions (slope estimate = 1.05, standard error = 0.04), suggesting that this fitted covariance model adequately described the c-ln EM spatial covariance structure. However,
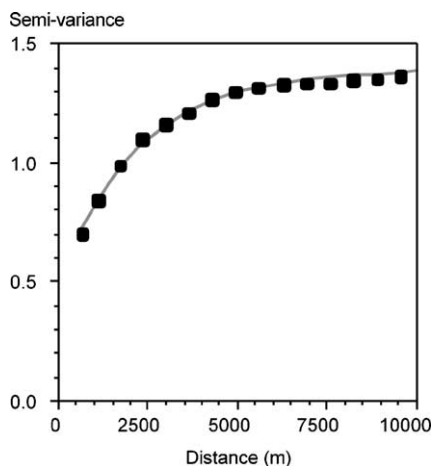
Fig. 13. Calculated variogram structure for the composite (c-ln EM) signal data, the best-fit isotropic exponential variogram model also shown.

the correlation between the observed and jack-knifed (cross-validated) predictions was only 0.69, due to the relatively large nugget effect present in this structure (e.g., about 35% of the total variability).

3.9. Generating the HSR model prediction map

Given the estimated covariance structure, the estimation of the hierarchical spatial model was complete. Specifically, the full model was specified as:

$$(y|z = z_0) = \beta_0 + \beta_1(z_0) + \beta_2(X_s) + \beta_3(Y_s) + \varepsilon \tag{13}$$

with $\varepsilon \sim iid\, N(0, \sigma^2 I)$; $z \sim \text{MVN}(z, \sigma_k^2 \Sigma)$ and where $y = \%$clay, $z = $c-ln EM, and the remaining variables are defined as before. To generate the map of the %clay estimates, we first interpolated the Z(c-ln EM) signal data onto a 100 by 100-m grid using an OK analysis. We then passed the resulting z_k predictions through the regression model in order to calculate the final $\hat{y}$ and Var$(y - \hat{y})$ estimates, using Eqs. (8.1) and (8.2). A map of the final predicted %clay pattern for the Trangie district is shown in Fig. 14. The coarsest sediments (i.e., %clay $\leq 35\%$) are for the most part located along the eastern margin of the district adjacent to the Macquarie River. Isolated patches of clay $\leq 35\%$ can also be seen adjacent to the Trangie Cowal. Typically, the %clay ranges between 35 and 40% next to the Cowal. This is similarly the case with the Old Alluvium (Meander Plain) Pedoderm, which runs parallel with the Mitchell Highway in the western part of the district. With respect to the landholdings located on the Trangie Cowal average clay% was slightly higher (i.e., 40–50%). The largest values of average %clay (i.e., $\geq 50\%$) are associated with the Old Alluvium (Meander Plain) and to the east and southeast of Buddah Lake. The area adjacent to Buddah Lake has the highest clay content. This is consistent with the contiguous area of Extragrades mapped
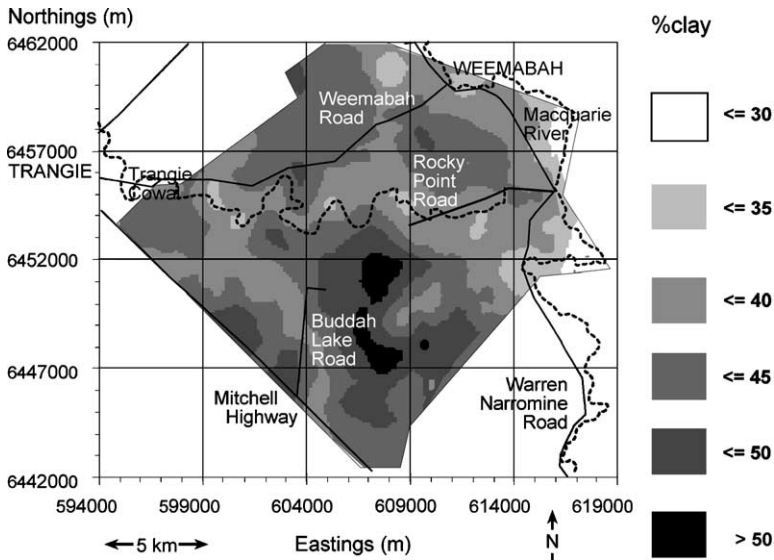
Fig. 14. Predicted average clay content to 7 m (%clay) map for the Trangie district of the lower Macquarie valley generated by the hierarchical spatial regression (HSR) model.

in Fig. 9, which sets apart this part of the landscape from the rest of the Old Alluvium (Meander Plain). It is also evident from Figs. 1 and 14 that most of the irrigated fields have been developed on the clayier sediments (i.e., clay content $\geq 40\%$). The major exceptions are some of the fields between the Weemabah and Rocky Point Roads. This is similarly the case with respect to the large earthen water reservoirs.

A map of the calculated standard deviation associated with these predictions is shown in Fig. 15. The white and darkest grey shaded areas indicate where the standard deviation was lowest (i.e., ≤ 6.5) and highest (i.e., >6.9), respectively. The highest standard deviations are associated with the south- and north-eastern margins of the study area is due to "edge effect" generally well known in the geostatistics community. The "edge effect" is caused by insufficient data at or close to the edge. Conversely, the standard deviation is lowest (≤ 6.5) in the central parts of the Trangie district.

3.10. Assessment of the HSR model accuracy and reliability

The reliability of the HSR model predictions were analyzed by (i) generating the %clay predictions at the eight independent validation sites and (ii) assessing the prediction accuracy at the 40 calibration sites using a cross-validation technique. Table 10 displays the measured and two types of predicted %clay estimates at the eight independent validation sites, respectively (see Fig. 11). The first column of predicted %clay values was generated using known c-ln EM signal data, while the second column of values was generated using estimated c-ln EM signal data (calculated via the OK analysis). The corresponding 95% confidence intervals were derived using the conditional [c-ln EM known, Eq. (7.2)] and un-
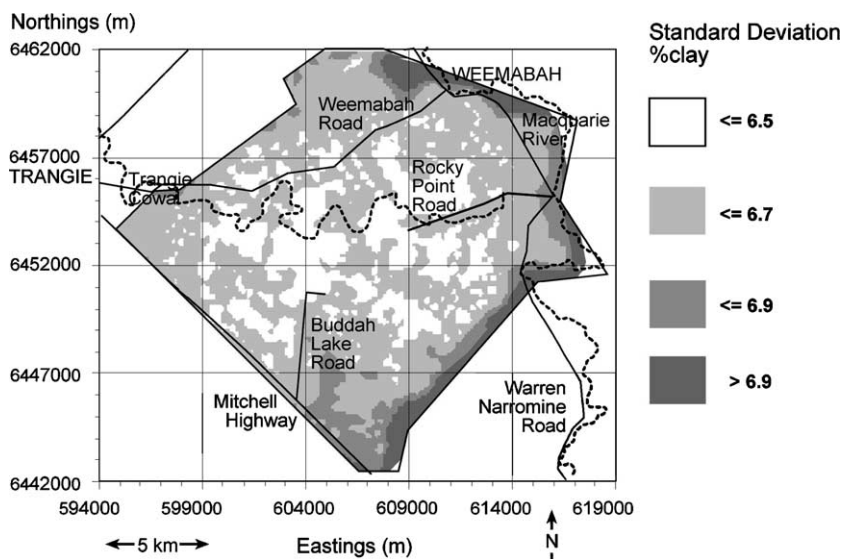
Fig. 15. Calculated standard deviation map (associated with average clay content to 7 m (%clay) predictions) generated by the hierarchical spatial regression (HSR) model.

conditional [c-ln EM estimated, Eq. (8.2)] hierarchical regression model variance formulas, respectively.

The first set of (conditional) %clay predictions agree reasonably well with the measured %clay values. The average predicted %clay level of 47.7% is close to the observed (true)

Table 10
Predicted average clay content to 7 m (%clay) estimates at eight validation sites (see Fig. 11 for locations), generated using known and estimated composite (c-ln EM) electromagnetic (EM) signal data

Validation ID	Measured (M)	Using known c-ln EM signal data, predicted (P)		Using estimated c-ln EM signal data, predicted (P)	
	%clay	%clay	95% CI	%clay	95% CI
(1) Measured vs. predicted					
41	57.4	49.9	(40.1, 59.7)	47.2	(34.1, 60.3)
42	59.9	54.5	(44.5, 64.4)	50.1	(36.9, 63.3)
43	44.4	45.1	(35.1, 55.0)	41.0	(27.9, 54.1)
44	37.2	39.1	(29.3, 48.9)	41.4	(28.3, 54.5)
45	40.4	42.3	(32.5, 52.1)	43.6	(30.3, 56.9)
46	46.2	50.6	(40.5, 60.6)	42.3	(29.2, 55.4)
47	57.6	54.9	(44.9, 64.9)	48.6	(35.5, 61.6)
48	36.0	45.3	(35.4, 55.2)	41.2	(28.1, 54.3)
(2) Root mean square error (RMSE)					
Average %clay	47.38	47.71		44.33	
Difference (M − P)		−0.34		2.95	
RMSE		5.08		6.73	
Corr(M, P)		0.88		0.92	

95% confidence limits for both sets of predictions also shown.

Table 11
Summary statistics for the conditional and unconditional average clay content to 7 m (%clay) predictions generated at the 40 calibration sample sites ($Z = c$-ln EM)

Variable	Mean	Standard deviation
$y = \%$clay	40.76	9.84
$u1 = $ prd %clay$\vert Z$ known	40.76	8.75
$u2 = $ prd %clay$\vert Z$ estimated	41.18	4.71
$y - u1$	0.000	4.503
$y - u2$	−0.420	8.726
Corr($y, u1$) = 0.89		
Corr($y, u2$) = 0.46		

average of 47.4%, and the observed versus prediction correlation estimate ($r = 0.88$) is very close to the square root of the regression model r^2-value (0.90). The second set of (unconditional) %clay predictions do not appear to agree as well with the measured data. The average predicted %clay level of 44.4% is farther away from the observed value, and the uncorrected root mean square error estimate is higher than the corresponding conditional estimate (6.73 versus 5.08). Interestingly, the observed versus unconditional predicted correlation estimate is quite high ($r = 0.92$). This latter result is atypical, and probably an artifact of the small validation sample size ($n = 8$).

Table 11 displays some basic results pertaining to both the conditional and unconditional predictions generated at the 40 calibration sites. In this table, the conditional (c-ln EM known) predictions are simply the predictions generated by Eq. (12). In contrast, the unconditional predictions were generated by replacing the known c-ln EM signal values in Eq. (12) with their corresponding cross-validation estimates. These results more clearly show the effect of using estimated (rather than known) signal data in the hierarchical regression model; the observed variance of the prediction distribution shrinks and the corresponding error variance increases. The expected correlation between the observed and predicted %clay must also decrease; in this cross-validation analysis the decrease is substantial (0.89 versus 0.46).

The significant reduction in the observed versus predicted %clay correlation estimate using estimated signal data is due to the increased uncertainty in these signal data estimates (see Figs. 4c–6c). This uncertainty is compounded by the large relative nugget effect seen in the c-ln EM variogram model (Fig. 13). This large nugget effect implies that the signal data is locally discontinuous, and thus precise interpolated signal readings (off the survey grid) cannot be generated using the kriging model. In contrast, the regression model appears to be reasonably accurate; the observed versus predicted %clay correlation estimate is 0.89. Hence, these results imply that the sampling density of the EM signal data needs to be increased (as opposed to increasing the number of %clay calibration samples) if more precise interpolated predictions are required.

3.11. Relationship between EM34 signal data, FKMe classes, and clay%

In order to better appreciate the relationship between the EM34 and EM38 signal data, %clay, FKMe classes and the clay stratigraphy of the Trangie district we describe the results
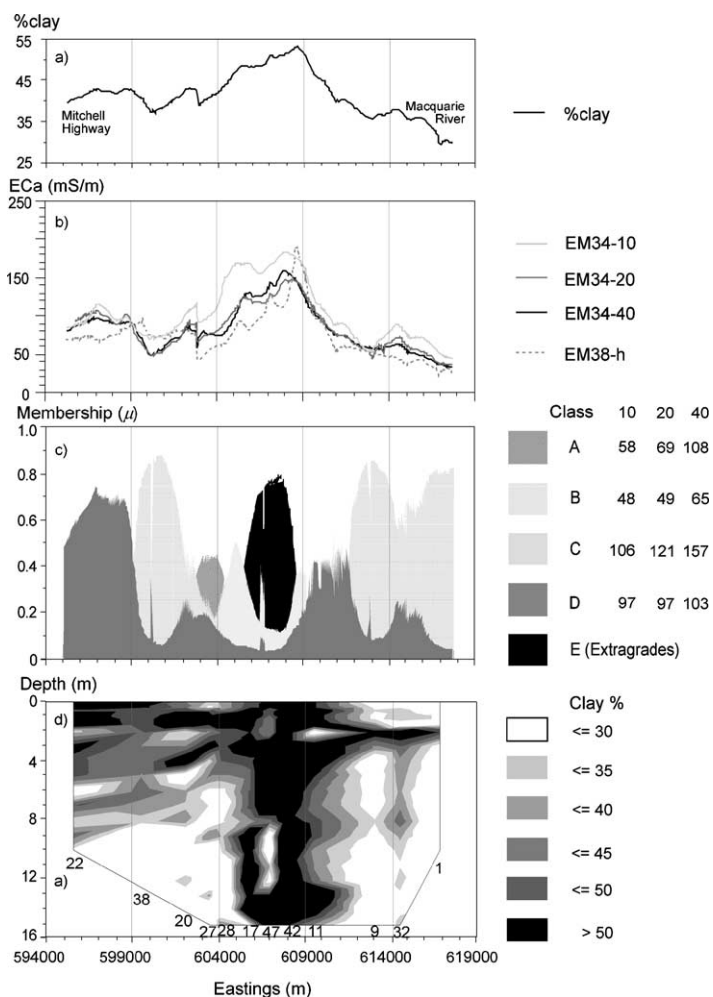
Fig. 16. Spatial distribution of: (a) %clay (i.e., average clay content to a depth of 7 m); (b) interpolated signal readings of the EM34 and EM38 (i.e., EM34-10, -20, and -40 m configurations and horizontal, respectively); (c) interpolated memberships (μ) for $c = 4 + 1$ Extragrade class; and (d) clay content with depth vs. Eastings (m).

along a detailed transect. Fig. 16 shows the data and results collected along an east–west transect situated at an approximate Northing of 6,452,000. Its location is shown in Fig. 3. With respect to Fig. 16d the clay % data comes from calibration profiles 22, 38, 20, 27, 28, 17, 47, 42, 11, 9, 32, and 1. Their approximate location along the traverse is also shown.

In order to understand the significance of the results we systematically describe them from east to west. Southeast of Trangie (Easting – 595,000) the EM34 signal readings (i.e., EM34-10, -20, and -40) are similar and generally range from 80 to 110 mS/m. These readings are equivalent to the centroids of Class D (i.e., 97, 97, and 103) and as shown

in Fig. 16c this portion of the traverse had the highest μ (i.e., 0.5–0.7) to this class. With respect to %clay, we would anticipate that the soil to a depth of 7 m would be about 42%. This is confirmed visually by the data presented in Fig. 16d. It indicates that the soil is medium clay (i.e., >45%) textured at depths of 0–2, 3–5, and at 7 m, while at 2 and 6 m it is generally a light to sandy clay (i.e., 30–40%). At an Easting of 60,000, %clay decreases slightly to 35%. This coincides with lower EM34 signal readings (i.e., 50, 50, and 70) that are consistent with the centroids of Class B. As shown in Fig. 16c this part of the traverse has high μ to this class (i.e., >0.8). From here until the middle portion of this traverse the signal readings could not be placed sufficiently well into any of the four regular classes although there is partial μ to Classes A and C.

At an Easting of 607,000, the EM34 signal readings were the highest recorded along the traverse and the Trangie district in general (see Figs. 4 and 5). With respect to the EM34-10 and EM34-20, the signal readings ranged between 130 and 150 mS/m, while the EM34-40 was greater than 150 mS/m. As shown in the legend of Fig. 16c, none of the class centroids coincide with these values. This is particularly the case with respect to the EM34-10 and EM34-20 readings. As a result the EM signal readings recorded across this part of the landscape could not be placed into any of the four regular classes (i.e., A, B, C, or D). This explains the large μ to the Extragrade class. This is consistent with the fact that this part of the district also had the highest %clay, which exceeds 45% (see Figs. 14 and 16a). The reason for the classification of this portion of the landscape to the Extragrade class becomes self-evident when considering results shown in Fig. 16d. Along this portion of the traverse the clay content to a depth of 15 m, generally exceeds 50%. In comparison to the rest of the traverse, and for that matter the Trangie district, this is atypical.

To the east of this clay dominated landscape there is some uncertainty in the FKMe classification. This is most likely attributable to the fact that all EM34 signal readings decrease quite markedly (100 mS/m) over a relatively short distance (i.e., 3 km) to values of 50–100 mS/m. The EM34 signal readings generally persist across most of the remainder of the traverse and are consistent with the centroids of Class B and to a lesser extent D. Here, the %clay is about 35% and is consistent with the %clay estimated along the eastern part of the transect where this class was represented. In terms of changes in clay content with depth there is much less stratification in this part of the landscape. What is worth noting is that at a depth of about 2 m there is a heavy clay layer underlying sandier sediments. Triantafilis et al. (2004) showed that deep drainage risk was high with respect to the sandier sediments. This is particularly the case when large earthen water reservoirs or conveyance channels, associated with irrigated agriculture, were constructed upon them. The higher underlying clay content goes some way in explaining why perched water tables can be problematic in this part of the landscape.

4. Summary and conclusions

The predominantly irrigated cotton-growing district located southeast of Trangie in the lower Macquarie valley of New South Wales was surveyed using EM38 and EM34 instruments. The EM38 survey (i.e., vertical EM38-v and horizontal EM38-h) generally reflected the known surface sediments of the Trangie district (i.e., Pedoderms – McKenzie,

1992). This was similarly the case with the EM34 at 10 m (EM34-10) and 20 m (EM34-20) configurations, although in some areas (e.g., Trangie Cowal between Weemabah and Rocky Point Roads) higher signal readings were consistent with isolated instances of point source soil salinization. With respect to the signal readings recorded with the EM34 in the 40 m (EM34-40) configuration, the results suggest that the instrument is influenced by deeper conductive anomalies including saline groundwater aquifers beneath the Gin Gin Hills (i.e., north of Weemabah Road) and water tables underlying the Trangie Cowal Pedoderm.

The FKMe analysis of the EM34 signal data (i.e., EM34-10, -20, and -40) confirmed these patterns by clustering similar signal readings into four regular and one Extragrade class. The use of the confusion index to map uncertainty in the clusters (FKMe) indicated areas where more information could be collected in order to improve the classification and understanding of the surface and subsurface hydrogeology. This is particularly the case in the central part of the study area where the CI was highest. We concluded that the most likely explanation for the higher uncertainty (i.e., $CI > 0.4$) is attributable to land use. In the first instance, dryland fields produce lower signal readings in the near surface (EM34-10) as compared with adjacent irrigated areas. Secondly groundwater recharge from irrigated areas cause soluble salts to accumulate beneath dryland areas. This results in higher signal readings in the deeper measurements (EM34-40). This situation is unique to the area and more detailed information is required to better understand the hydrology and best management.

Nevertheless, the FKMe classes produced generally reflect the known Pedoderms and hydrogeology of the Trangie district. The FKMe classification, therefore, provided a useful blocking strategy for site selection. However, the combined FKMe and SSRS design did not lead to different regression relationships for each class. We conclude that mineralogical differences do not influence the EM34. As a result, we developed a homogeneous regression model to estimate %clay across the Trangie district. This was achieved by determining a hierarchical spatial regression model, which included two trend surface parameters (i.e., Eastings and Northings) and testing significance of five-signal readings by using a forward sequential selection procedure. We found that the natural log (ln) of the sum of the EM38-h, EM34-10, and EM34-40 signal readings, along with the Easting and Northing would provide the most parsimonious combination. We conclude that the EM38-h best accounts for the variation in the surface sediments (0–1 m), while the EM34-10 and EM34-40 provide information relating to the vadose zone (1–7 m).

The HSR modeling approach used in this analysis has two advantages over co-kriging. The first of these is that the HSR approach avoids the task of developing cross-covariance models that can be time-consuming. Secondly, the approach allows one to model and test multiple inter-dependence structures (i.e., as illustrated during FKMe analysis) between the predictor variables. Like co-kriging, the final result is still an interpolated map that describes the spatial distribution of average clay content to 7 m (%clay). The %clay map compliments the results achieved by McKenzie (1992) using a more conventional approach (i.e., using broad scale ecological and geomorphological information, monochrome aerial photographs, and geological and topographic maps).

In terms of decreasing the prediction variance there are several choices. The first is decreasing the ground-based EM survey interval from 500 to 250 or even 125 m. Although this would be a time-consuming proposition, the information would be useful in improving the cause and management of soil and water salinization in the irrigated cotton-growing areas

associated with the Trangie Cowal (Alluvial Plain). Alternatively, airborne EM systems could be deployed to increase the EM survey resolution, or other types of ancillary information (i.e., gamma radiometric, LANDSAT, RADARSAT, etc.) that might be incorporated into the modeling process. For example, a combined FKM analysis of the EM34, EM38, and remotely sensed information might provide better distinction of surface sediments and delineation of robust soil management units using a quantitative approach as described herein.

Acknowledgements

Appendix A. List of abbreviations

clay%   average clay content to 7 m depth
EC_a apparent soil electrical conductivity
EM   electromagnetic (EM) induction
EM34-10 EM34 signal reading at 10 m coil configuration (horizontal dipole mode)
EM34-20 EM34 signal reading at 20 m coil configuration (horizontal dipole mode)
EM34-40 EM34 signal reading at 40 m coil configuration (horizontal dipole mode)
EM38-v   EM38 signal reading in vertical dipole mode
EM38-h   EM38 signal reading horizontal dipole mode
c-ln EM ln(EM34-10) + ln(EM34-40) + ln(EM38-h)
FKM   fuzzy *k*-means
FKMe   fuzzy *k*-means with extragrades
OK   ordinary kriging
SRSS   spatial response surface sampling
HSR   hierarchical spatial regression

References

Aitchison, J., 1986. The Statistical Analysis of Compositional Data. Chapman Hall, London, UK.
Bezdek, J.C., 1981. Pattern Recognition with Fuzzy Objective Function Algorithms. Plenum Press, New York, NY, USA.

Box, G.E.P., Draper, N.R., 1987. Empirical Model-Building and Response Surfaces. John Wiley, New York, NY, USA.

Brandsma, A.S., Ketellapper, R.H., 1979. Further evidence on alternative procedures for testing of spatial auto-correlation amongst regression disturbances. In: Bartels, C.P.A., Ketellapper, R.H. (Eds.), Exploratory and Explanatory Statistical analysis of Spatial Data. Martinus Nijhoff, Hingham, MA, pp. 113–136.

Bresler, E., Dagan, G., Wagenet, R.J., Laufer, A., 1984. Statistical analysis of salinity and texture effects on spatial variability of soil hydraulic properties. Soil Sci. Soc. Am. J. 48, 16–25.

Brus, D.J., Knotters, M., van Dooremolen, P., van Kernebeek, P., van Seeters, R.J.M., 1992. The use of electro-magnetic measurements of apparent soil electrical conductivity to predict the boulder clay depth. Geoderma 84, 79–84.

Burrough, P.A., Van Gaans, P.F.M., Hootsmans, R., 1997. Continuous classification in soil survey: spatial corre-lation, confusion and boundaries. Geoderma 77, 115–135.

Corwin, D.L., Kaffka, S.R., Hopmans, J.W., Mori, Y., van Groenigen, J.W., van Kessel, C., Lesch, S.M., Lesch, J.D., 2003. Assessment of field-scale mapping of soil quality properties of a saline-sodic soil. Geoderma 114, 231–259.

Davey, B.G., 1990. The chemical properties of soils. In: Campbell, K.O., Bowyer, J.W. (Eds.), Scientific Basis of Modern Agriculture. Sydney University Press, Sydney, Australia (Chapter 4).

De Gruijter, J.J., McBratney, A.B., 1988. A modified fuzzy *k*-means method for predictive classification. In: Bock, H.H. (Ed.), Classification and Related Methods of Data Analysis. Elsevier, Amsterdam, pp. 97–104.

Frenkel, H., Goertzen, J.O., Rhoades, J.D., 1978. Effects of clay type and content, exchangeable sodium percentage, and electrolyte concentration on clay dispersion and soil hydraulic conductivity. Soil Sci. Soc. Am. J. 42, 32–39.

Gallichand, J., Marcotte, D., 1993. Mapping clay content for subsurface drainage in the Nile Delta. Geoderma 58, 165–179.

Goovaerts, P., 1999. Geostatistics in soil science: state-of-the-art and perspectives. Geoderma 89, 1–45.

Jabro, J.D., 1992. Estimation of saturated hydraulic conductivity of soils from particle size distribution and bulk density data. Trans. ASAE 35, 557–560.

Kalivas, D.P., Kollias, V.J., 1999. Mapping topsoil clay content of a region in Central Greece using two empirical methods. Agric. Medit. 129, 117–127.

Kitchen, N.R., Sudduth, K.A., Drummond, S.T., 1996. Mapping of sand deposition from 1993 midwest floods with electromagnetic induction measurements. J. Soil Water Conserv. 51, 336–340.

Knotters, M., Brus, D.J., Oude Voshaar, J.H., 1995. A comparison of kriging combined with regression for spatial interpolation of horizon depth with censored observations. Geoderma 67, 227–246.

Lagacherie, P., Cazermier, D.R., van Gaans, P.F.M., Burrough, P.A., 1997. Fuzzy *k*-means clustering of fields in an elementary catchment and extrapolation to a larger area. Geoderma 77, 197–216.

Lesch, S.M., Strauss, D.J., Rhoades, J.D., 1995a. Spatial prediction of soil salinity using electromagnetic induction techniques. 1: Statistical prediction models: a comparison of multiple linear regression and cokriging. Water Resour. Res. 31, 373–386.

Lesch, S.M., Strauss, D.J., Rhoades, J.D., 1995b. Spatial prediction of soil salinity using electromagnetic in-duction techniques. 2: An efficient spatial sampling algorithm suitable for multiple linear regression model identification and estimation. Water Resour. Res. 31, 387–398.

Lesch, S.M., 2005. Sensor-directed response surface sampling designs for characterizing spatial variation in soil properties. Comp. Electron. Agric. 46, 153–179.

Littell, R.C., Milliken, G.A., Stroup, W.W., Wolfinger, R.D., 1996. SAS System for Mixed Models. SAS Institute Inc., Cary, NC, USA.

Mapa, R.B., Kumaragamage, D., 1996. Variability of soil properties in a tropical Alfisol used for shifting cultivation. Soil Technol. 9, 187–197.

McBratney, A.B., Webster, R., 1981. The design of optimal sampling schemes for local estimation and mapping of regionalized variables. II. Program and examples. Comput. Geosci. 7, 335–365.

McBratney, A.B., Moore, A.W., 1985. Application of fuzzy sets to climatic classification. Agric. For. Meteor. 35, 165–185.

McBratney, A.B., De Gruijter, J.J., 1992. A continuum approach to soil classification and mapping: classification by modified fuzzy *k*-means with extragrades. J. Soil Sci. 43, 159–175.

McBratney, A.B., De Gruijter, J.J., Brus, D.J., 1992. Spatial prediction and mapping of continuous soil classes. Geoderma 54, 39–64.

McBratney, A.B., Hart, G.A., McGarry, D., 1991. The use of region partitioning to improve the representation of geostatistically mapped soil attributes. J. Soil Sci. 42, 513–532.

McKenzie, N.J., 1992. Soils of the Lower Macquarie Valley, New South Wales. CSIRO Division of Soils, Divisional Report no. 117. Canberra, Australia.

McNeill, J.D., 1980, Electromagnetic terrain conductivity measurement at low induction numbers. Technical Note TN-6. Geonics Limited, Ont., Canada.

McNeill, J.D., 1990. Geonics EM38 Ground Conductivity Meter: EM38 Operating Manual. Geonics Limited, Ont., Canada.

Minasny, B., McBratney, A.B., 2002. FuzME version 3.0. Australian Centre for Precision Agriculture. The University of Sydney, Australia, http://www.usyd.edu.au/su/agric/acpa.

Myers, R.H., 1986. Classical and Modern Regression with Applications. Duxbury Press, Boston, MA, USA.

Nathan, G., 1988. Inference based on data from complex sample designs. In: Krishnaiah, P.R., Rao, C.R. (Eds.), Handbook of Statistics, vol. 6. Elsevier, Amsterdam, The Netherlands (Chapter 10).

Oberthur, T., Goovaerts, P., Dobermann, A., 1999. Mapping soil texture classes using field texturing, particle size distribution and local knowledge by both conventional and geostatistical methods. Eur. J. Soil Sci. 50, 457–479.

Odeh, I.O.A., McBratney, A.B., Chittleborough, D.J., 1992a. Soil pattern recognition with fuzzy c-means: application to classification and soil landform interrelationships. Soil Sci. Soc. Am. J. 56, 505–516.

Odeh, I.O.A., McBratney, A.B., Chittleborough, D.J., 1992b. Fuzzy c-means and kriging for mapping soil as a continuous system. Soil Sci. Soc. Am. J. 56, 1848–1854.

Odeh, I.O.A., McBratney, A.B., 2000. Using AVHRR images for spatial prediction of clay content in the lower Namoi Valley of eastern Australia. Geoderma 97, 237–254.

Odeh, I.O.A., McBratney, A.B., Chittleborough, D.J., 1995. Further results on prediction of soil properties from terrain attributes: heterotopic cokriging and regression-kriging. Geoderma 67, 215–226.

Odeh, I.O.A., Todd, A.J., Triantafilis, J., 2003. Spatial prediction of particle size fractions as compositional data. Soil Sci. 168, 501–515.

Ohashi, Y., 1984. Fuzzy clustering and robust estimation. In: 9th meeting SAS Users group International, Hollywood Beach, Florida, pp. 18–21.

Pawlowsky, V., 1984. On spurious spatial covariance between variables of constant sum. Sci. de la Terre Inf. Geol. 21, 107–113.

Press, W.H., Tuekolsky, S.A., Vetterling, W.T., Flannery, B.P., 1992. Numerical Recipes: The Art of Scientific Computing. Cambridge University Press, Cambridge, UK.

Rayment, G.E., Higginson, F.R., 1992. Australian Laboratory Handbook of Soil and Water Chemical Methods. Australian Soil and Land Survey Handbook. Inkata Press, Melbourne.

Roubens, M., 1982. Fuzzy clustering algorithms and their validity. Eur. J. Oper. Res. 10, 294–301.

Royle, J.A., Berliner, L.M., Wikle, C.K., Milliff, R., 1998. A hierarchical spatial model for constructing wind fields from scatterometer data in the Labrador Sea. In: Case Studies in Bayesian Statistics. Springer-Verlag, New York, NY, USA, pp. 51–75.

Royle, J.A., Berliner, L.M., 1999. A hierarchical approach to multivariate spatial modelling and prediction. J. Agric. Biol. Environ. Stat. 4, 29–56.

Russell, E.W., 1973. Soil Conditions and Plant Growth, 10th ed. Longman Group Limited, London, UK.

SAS, 1990. SAS User's Guide: Statistics, Version 6, 4th ed. SAS Institute, Cary, NC, USA.

Sudduth, K.A., Kitchen, N.R., Hughes, D.F., Drummond, S.T., 1995. Electromagnetic induction sensing as an indicator of productivity on claypan soils. In: Probert, P.G., Rust, R.I.H., Larson, W.E. (Eds.), Proceedings of the Second International Conference on Site Specific Management for Agricultural Systems. Minneapolis, MN, USA, pp. 671–681.

Shapiro, S.S., Wilk, M.B., 1965. An analysis of variance test for normality (complete samples). Biometrika 52, 591–611.

Thompson, S.K., 1992. Sampling. John Wiley, New York, NY, USA.

Triantafilis, J., Huckel, I.A., Odeh, I.O.A., 2001a. Comparison of statistical prediction methods for estimating field-scale clay content using different combinations of ancillary variables. Soil Sci. 166, 415–427.

Triantafilis, J., Ward, W.T., Odeh, I.O.A., McBratney, A.B., 2001b. Creation and interpolation of continuous soil layer classes in the lower Namoi valley. Soil Sci. Soc. Am. J. 65, 403–413.

Triantafilis, J., Ahmed, M.F., Odeh, I.O.A., 2002. Application of a mobile electromagnetic sensing system (MESS) to assess cause and management of soil salinization in an irrigated cotton-growing field. Soil Use Manage. 18, 330–339.

Triantafilis, J., Huckel, A.I., Odeh, I.O.A., 2003a. Field-scale assessment of deep drainage risk. Irrig. Sci. 21, 183–192.

Triantafilis, J., Odeh, I.O.A., Minasny, B., McBratney, A.B., 2003b. Elucidation of physiographic and hydrogeological units using fuzzy *k*-means classification of EM34 data in the lower Namoi valley. Environ. Mod. Soft. 18, 667–680.

Triantafilis, J., Odeh, I.O.A., Jarman, A.L., Short, M., Kokkoris, E., 2004. Estimating and mapping deep drainage risk at the district level in the lower Gwydir and Macquarie valleys. Australia. Aust. J. Exp. Agric. 44, 893–912.

Vauclin, M., Vieira, S.R., Vauchad, G., Nielsen, D.R., 1983. The use of cokriging with limited field soil observations. Soil Sci. Soc. Am. J. 47, 175–184.

Vaughan, P.J., Lesch, S.M., Corwin, D.L., Cone, D.G., 1995. Water content effect on soil salinity prediction: a geostatistical study using cokriging. Soil Sci. Soc. Am. J. 59, 1146–1156.

Voltz, M., Webster, R., 1990. A comparison of kriging, cubic splines and classification for predicting soil properties from sample information. J. Soil Sci. 41, 473–490.

Valliant, R., Dorfman, A.H., Royall, R.M., 2000. Finite Population Sampling: A Prediction Approach. John Wiley, New York, NY, USA.

Wackernagel, H., 1995. Mulitvariate Geostatistics: An Introduction with Applications. Springer-Verlag, Berlin Heidelberg, Germany.

Van Groenigen, J.W., Siderius, W., Stein, A., 1999. Constrained optimisation of soil sampling for minimisation of the kriging variance. Geoderma 87, 239–259.

Walvoort, J.J., De Gruijter, J.J., 2001. Compositional kriging: a spatial interpolation method for compositional data. Math. Geol. 33, 951–966.

Weisberg, S., 1985. Applied Linear Regression. John Wiley, New York, NY, USA.

Williams, B.G., Arunin, S., 1990. Inferring recharge/discharge areas from multi-frequency electromagnetic induction measurements, CSIRO Tech. Memo. 90/11. CSIRO Division of Water Resources, Canberra, Australia.

Williams, B.G., Baker, G.C., 1982. An electromagnetic induction technique for reconnoissance surveys of soil salinity hazards. Aust. J. Soil Res. 20, 107–118.

Williams, B.G., Hoey, D., 1987. The use of electromagnetic induction to detect the spatial variability of the salt and clay contents of soil. Aust. J. Soil Res. 25, 21–28.

Zhang, R., Warrick, A.W., Myers, D.E., 1992. Improvement of the prediction of soil particle size fractions using spectral properties. Geoderma 52, 223–234.